University of South-Eastern Norway

www.usn.no

FMH606 Master's Thesis 2024

Process Technology

Experimental study of deflagration to detonation transition of hydrogen-air gas explosion

Attanayake Mudiyanselage Chinthaka Attanayake

Faculty of Technology, Natural sciences and Maritime Sciences
Campus Porsgrunn

University of South-Eastern Norway

www.usn.no

Course: FMH606 Master's Thesis, 2024

Title: Experimental study of DDT of hydrogen-air gas explosion

Number of pages: 66

Keywords: DDT, flame propagation, hotspot, detonation

Student: Attanayake Mudiyanselage Chinthaka Attanayake

Supervisor: Associate Prof. Mathias Henriksen, Prof. Dag Bjerketvedt, and Peter Bosnic

External partner: Hydrogeni (FME Research Center)

Summary:

Hydrogen is emerging as a promising alternative fuel to fossil-based fuels, and it will play an important role in a carbon-neutral future. However, storing and transporting hydrogen poses a challenge due to the high risk of explosion. Hydrogen-air mixtures have a higher detonability, and explosions could transition from deflagration to detonation. The reason behind this phenomenon is important to address risks and safety concerns.

The study aimed to examine the deflagration to detonation transition (DDT) for hydrogen-air-premixed gas. The experiments were conducted in a one-meter channel as a laboratory experiment. The experiments were conducted for equivalence ratios of 0.8 to 1.5. The results and findings of maximum peak pressures, flame front velocities, and images from high-speed cameras were analyzed to understand DDT. DDT was observed only for the equivalence ratio 1.1 with a 15% probability. A hotspot formation was observed for every detonated case. Flame front velocities were observed between 1800 ms^{-1} and 2000 ms^{-1} for detonated cases. The highest average peak pressures were observed for the equivalence ratios 1.0 to 1.3.

Preface

This master's thesis work carried out in the spring of 2024 at the University of South-Eastern Norway (USN), Porsgrunn. This was conducted as a part of the Master of Science degree at USN.

The main objective of this study was to conduct explosion experiments for hydrogen-air-premixed gas to examine the DDT. Hydrogeni (FME Research Center) is an external partner on this project.

The thesis was supervised by Associate Prof. Mathias Henriksen, Prof. Dag Bjerketvedt, and PhD scholar Peter Bosnic, with whom I have learned and improved my knowledge and skills during this thesis.

First, I would like to express my sincere gratitude to Associate Professor Mathias Henriksen, my supervisor and Professor Dag Bjerketvedt, my co-supervisor, who guided me throughout the thesis. I would especially like to thank them for their valuable time giving me advice, and providing me with motivation and guidance. I would like to thank Peter Bosnic, my thesis co-supervisor, who was always support me whenever I needed it. His keen observations, knowledge, guidance, and support motivated me to work harder.

I would also like to thank the staff of the USN library for their support whenever I needed it.

I thank my friends who supported me during the thesis work.

Finally, I would like to thank my family, who constantly encouraged me and supported me in doing my best to complete this thesis.

Porsgrunn, 30.05.2024

Attanayake Mudiyanselage Chinthaka Attanayake

Contents

1 Introduction 9
1.1 Hydrogen characteristics and safety overview 9
1.1.1 Accidents and incidents *9*
1.2 Aim of the study 10
1.3 Thesis structure 11
2 Literature review 12
2.1 Flame propagation and its relationship with DDT 12
2.1.1 Laminar flame propagation *13*
2.1.2 Flame instabilities *14*
2.1.3 Turbulent flame propagation *16*
2.2 Detonation 18
2.3 Deflagration to detonation transition (DDT) 20
2.3.1 Deflagration to detonation transition (DDT) *20*
2.3.2 Experimental studies of explosions in channels on DDT *21*
3 Experiments 24
3.1 Experimental setup 24
3.2 Experimental procedure 26
3.3 Experimental matrix 26
4 Results and discussion 29
4.1 Pressure and highspeed image data analysis 29
4.1.1 Pressure data analysis *29*
4.1.2 Highspeed image data analysis *37*
4.2 Comparison and validation 47
4.3 Error sources 48
5 Conclusion 51
6 Suggestions for future study 52

Nomenclature

Symbol	Expression	Unit
A	Area	m^2
ρ	Density	kg/m^3
C_p	Heat capacity	J/K
λ	Heat conductivity	W/m K
S_L	Laminar burning velocity	m/s
Le	Lewis number	-
D	Molecular diffusivity	m^2/s
$\dot{m}$	Rate of fuel consumption	kg/s
α	Thermal diffusivity	m^2/s
u_o'	Turbulent intensity	-

Abbreviations

AC	Alternating current
CFD	Computational fluid dynamics
CJ	Chapman-Jouguet
DDT	Deflagration to detonation transition
IEA	International Energy Agency
RMS	Root mean square
TNT	Trinitrotoluene
ZND	Zel'dovich, von Neumann and Döring

Overview of figures and tables

List of figures

Figure 2.1: Combustion regimes during flame development from ignition to detonation in premixed gas explosion [13] 12

Figure 2.2: Premixed flame propagation in a duct [14] 13

Figure 2.3: Mechanism of the Landau-Darrieus instability [19] 15

Figure 2.4: Illustration of Rayleigh-Taylor instability [20] 15

Figure 2.5: Diagram of premixed turbulent combustion regimes [18] 17

Figure 2.6: Change of physical properties of s ZND detonation wave [21] 19

Figure 2.7: Sketch of triple point and detonation cell structure [24] 20

Figure 2.8: Various transition to detonation modes observed in $2H2 + O2$ mixtures by Urtview and Oppenheim [21], [27]. (a) detonation occurring between flame and shock, (b) detonation occurring at flame front, (c) detonation occurring at shock front, (d) detonation occurring at contact discontinuity 21

Figure 3.1: Schematic illustration of the experimental setup [10]. 24

Figure 3.2: Explosion channel used in this experiment 25

Figure 4.1: Pressure sensor readings of the explosion experiment P105_T00001 (the equivalence ratio is 1.1) 32

Figure 4.2: Flame position with the time for the experiment in Figure 4.1. A: Flame propagation before obstacles, B: Flame propagation after flame reaching the obstacles. 34

Figure 4.3: Channel section one pressure readings at pressure sensor two for equivalence ratio 1.1 during the flame propagation A) experiments after the repair, B) experiments before the repair 35

Figure 4.4: Maximum overpressures at pressure sensor one during laminar flame propagation for all experiments in Table 4.1 36

Figure 4.5: P107_T0018 pressure readings at pressure sensor one, flame position, and flame velocity during laminar flame propagation A) graphs of pressure at pressure sensor one and flame position during flame propagation in channel section one, B) graphs of flame front velocities calculated from raw measurements, filtered flame front velocities, and third-degree polynomial fitted velocities 38

Figure 4.6: Flame front velocity in channel section one for the experiments done for the equivalence ratio of 0.9 39

Figure 4.7: Flame front velocity in channel section one for the experiments done for the equivalence ratio of 1.0 40

Figure 4.8: Time taken by flame fronts to reach the obstacles in experiments with equivalence ratios 0.9 and 1.0 40

Figure 4.9: Flame front velocities during the laminar flame propagation for experiments with DDT 41

Figure 4.10: P107_T0018 pressure readings, flame front velocity, and flame front position during flame propagation in channel section two, A) pressure readings at pressure sensors 2, 3, and 4, B) Flame front position and flame front velocity..... 42

Figure 4.11: Flame front velocity along the channel in channel section two for the experiments done for the equivalence ratio of 0.9 43

Figure 4.12: Flame front along the channel in channel section two for experiments done for equivalence ratio 1.0 43

Figure 4.13: Flame front velocities along the channel in channel section two for experiments with DDT 44

Figure 4.14: Kirana images for the flame propagation before the obstacles 45

Figure 4.15: Flame propagation in channel section two for the experiments where detonations were observed during P106. a) P106_T00002, b) P106_T00003, c) P106_T00004 46

Figure 4.16: Flame propagation in channel section two for the experiments where detonations were observed during P103 and P107. d) P103_T00007, d) P107_T00018..... 47

Figure 4.17: Hydrogen concentration test results for equivalence ratio 1.1 49

Figure 4.18: Hydrogen concentration test results for equivalence ratio 1.3 50

List of tables

Table 3.1: Experimental matrix. 27

Table 3.2: Tabel for details on experiments (project number-based) 27

Table 4.1: Table for details on the number of experiments used for the data analysis. 29

Table 4.2: Peak pressure analysis for deflagration and detonation experiments 30

Table 4.3: Peak pressure comparison for the experiments before and after the repair 31

Table 4.4: Average maximum pressure at pressure sensor one during laminar flame propagation 36

1 Introduction

The thesis addresses the deflagration-to-detonation transition (DDT) in a hydrogen-air-premixed gas explosion. The introduction chapter focuses on the background that motivated this study, its aim, and its report structure.

1.1 Hydrogen characteristics and safety overview

Hydrogen is a colorless, odorless, tasteless, and flammable substance found to be a diatomic gas. Hydrogen is a very light gas, and due to its' high energy content and emission-free burning, it has become a prime prospect as an energy carrier [1]. According to IEA's global hydrogen review and global energy outlook [2], hydrogen is on the way to becoming the next prominent energy carrier. In this process, hydrogen should be transported across regions and continents. However, transporting hydrogen comes with its own risks due to the high risk of flammability and explosion hazards.

Hydrogen is transported as a liquid at extremely low temperatures or compressed gas at high pressures. However, alternative methods are developing, such as ammonia. Handling hydrogen is involved in every alternative, so studying the safety aspects of hydrogen-premixed gas is vital for the future energy industry. Hydrogen leaks can cause explosions, which can propagate into detonations that have serious consequences and cause severe damage.

1.1.1 Accidents and incidents

There are many recorded accidents and incidents in history where detonations have occurred. Few major cases have been recorded of gas explosions that have transitioned to detonations. A few of those accidents are mentioned in this section.

1.1.1.1 Explosion in Port Hudson

The explosion in Port Hudson is one of the incidents where an explosion transitioned into a detonation. This incident happened in 1970. Burgess and Zabetakis [3], in their report on the Port Hudson explosion, conclude that an initial leak in a liquid propane pipeline turns into an explosion that transitions to detonation. The report shows that the detonation had happened due to a propane and air cloud distributing around 40000 m2. The total reported liquid propane loss due to the leak, the explosion, and the fire after the explosion was over 700000 liters. The energy released by the explosion is equivalent to 50 tons of detonating TNT. The effects of the explosion could be experienced even 15 miles away from the explosion. Following the detonation, afterburning is described as a firestorm, according to the study of Burgess and Zabetakis [3].

1.1.1.2 Explosion in ammonia plant in Porsgrunn

The explosion in an ammonia plant in Porsgrunn, Norway, is one of the accidents involving hydrogen. This happened in 1985 due to a hydrogen leak in the plant. Bjerketvedt and Mjaavatten [4] concluded in their study that around 10 to 20 kg of hydrogen had leaked and around 3.5 to 7 kg of hydrogen burned during the explosion. However, there was no quantitative evidence of a detonation occurrence. However, considering the damages, the study

concludes that the explosion is most likely a detonation. The effects of this explosion could be seen around 700 m from the explosion.

1.1.1.3 Buncefield explosion

This happened in 2005 at the Buncefield fuel storage site in the UK due to an overfilling of winter-grade gasoline. Bradley et al. [5] analyzed the explosion, which released approximately 300 tons of gasoline, and concluded that there was not enough evidence to confirm DDT. However, the study has details on how flame acceleration and turbulence can cause DDT.

1.1.1.4 Hydrogen-related accidents

Many hydrogen-related accidents have been reported recently. A hydrogen explosion in Sandvika, Norway, in 2019 [6] and a hydrogen explosion at a power plant in Muskingum, Ohio, in 2007 [7] are recent hydrogen-related explosions. However, the Fukushima nuclear power plant incident also recorded some gas explosions [8], which most likely were due to the hydrogen released from the reactor.

Hydrogen-related accidents are increasing due to its high usage as an energy carrier. When released, hydrogen easily gets mixed with air, and premixed explosions can propagate into detonations, which can create fatal consequences. Thus, studying hydrogen explosions and DDT is an important study area.

1.2 Aim of the study

Gas explosions can have severe consequences that potentially cause damage to human lives, the environment, and properties. Understanding explosions and flame propagation is critical to addressing safety measures, and flame propagation is one of the key reasons for DDT. Thus, experimenting with these phenomena is crucial. Flame propagation through channels has been studied by many using pressure, temperature, and highspeed imaging data for different gases and gas mixtures. Largescale experiments are expensive and complicated to do repetitively due to the difficulty of arranging and performing. Lab-scale experiments and simulations are easier to perform repetitively.

Computational fluid dynamic (CFD) simulations are based on mathematical models, which are discretized and solved numerically to analyze a phenomenon. However, experiments are needed to validate these simulations and models. Thus, lab-scale experiments will be used to understand the theories and validations. Since lab-scale experiments are easy to perform repetitively, they can be used to understand phenomena like DDT. DDT can happen for many reasons; thus, it is important to understand the reasons behind its occurrence.

This study aims to understand the deflagration-to-detonation transition (DDT) in a one-meter obstructed channel. Initially, the task was to examine DDT in this channel; however, during the experiments, DDT did not occur as predicted. Henriksen et al. [9] have observed a 50% probability during the experiments in the same setup. Thus, the objective of the study has changed to examine the reasons for the lower number of DDT. A literature review on DDT of hydrogen-air explosions was done during the study to understand the study area. Experiments were conducted on hydrogen-air explosions in the laboratory, and the experimental results were further processed using Python. Findings from the processed results were presented and discussed.

1.3 Thesis structure

The report contains six chapters. The first chapter gives the background that motivated this study and its aim. The second chapter contains a literature review on flame propagation and DDT. The third chapter contains all the methods and procedures followed during experiments and the analysis of the results. The fourth chapter presents the results, discusses the findings, and compares them with previous studies. The fifth chapter concludes the study, and the sixth chapter contains the future study areas.

2 Literature review

This chapter reviews theories and previous studies on hydrogen safety, hydrogen explosions, and DDT of premixed gas and air mixtures. As mentioned previously, gas explosions have severe consequences. Many have studied flame propagation using pressure, temperature, and high-speed imaging data on explosions and combustion for different gases and gas mixtures to find solutions to mitigate severe consequences [8], [9], [10], [11], [12], [13].

2.1 Flame propagation and its relationship with DDT

This thesis focuses on flame propagation inside a transparent obstructed channel and analyzes the pressure and high-speed imaging data to examine DDT. Many studies have used a similar method [8], [11], [13]. Henriksen et al. [9], [10], [12] have used a similar setup in the study of flame propagation and DDT.

Knudsen [13] did explosion experiments on a single obstructed pipe with a 107 mm inner diameter for hydrogen, hydrogen, and carbon monoxide mixture, propane, and methane premixed with air, and observed DDT for hydrogen and air mixtures. This study reviews the transition to detonation as seen in previous studies and identifies that flame propagation is an essential aspect of DDT. Figure 2.1 shows how the premixed combustion evolves into a detonation from ignition.

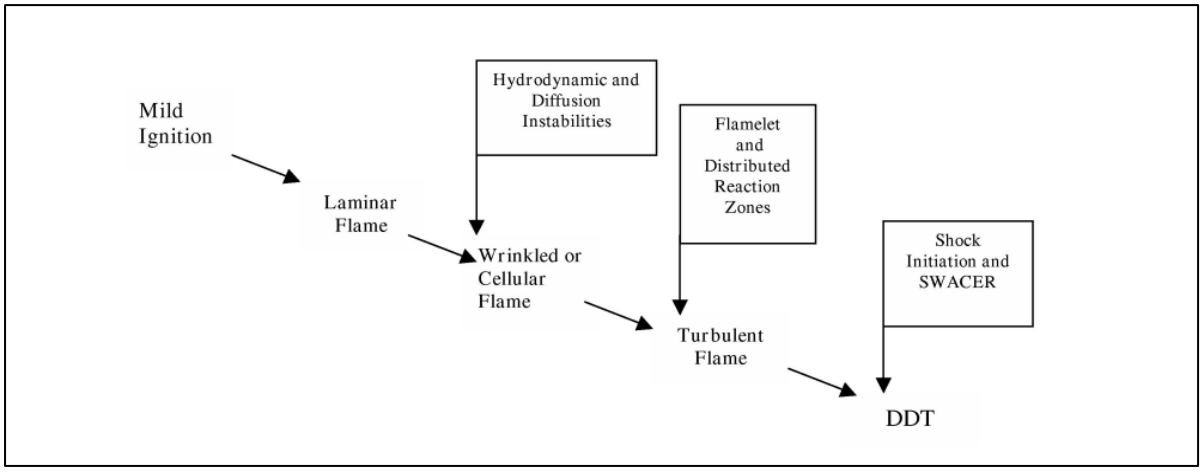

Figure 2.1: Combustion regimes during flame development from ignition to detonation in premixed gas explosion [13]

The current explosion study uses premixed combustion. It happens in different regimes related to explosions and flame propagation, which can be described as laminar, turbulent, or detonations. Ignition is the initiation of combustion.

Ignition can be identified in two ways: auto ignition and piloted ignition. In auto ignition, reactants achieve self-heating and reach the required temperature for combustion, while in piloted ignition, an external source starts the combustion [14]. In this study, pilot ignition was performed using a spark. The next evolution after the ignition is a laminar flame.

2.1.1 Laminar flame propagation

The premixed laminar flame structure has several regions. They are unburned fuel and air; preheat zone, where the fuel-air is preheated before the combustion reaction; reaction zone, where the mixture releases energy by combustion while visible as a flame; and burned gases, where products of the combustion reaction are released. The flame, or the reaction zone, is a thin layer that has several reaction layers where oxidation and radical formation happen, and radical consumption occurs at the inner layers [13], [14]. This is shown in Figure 2.2.

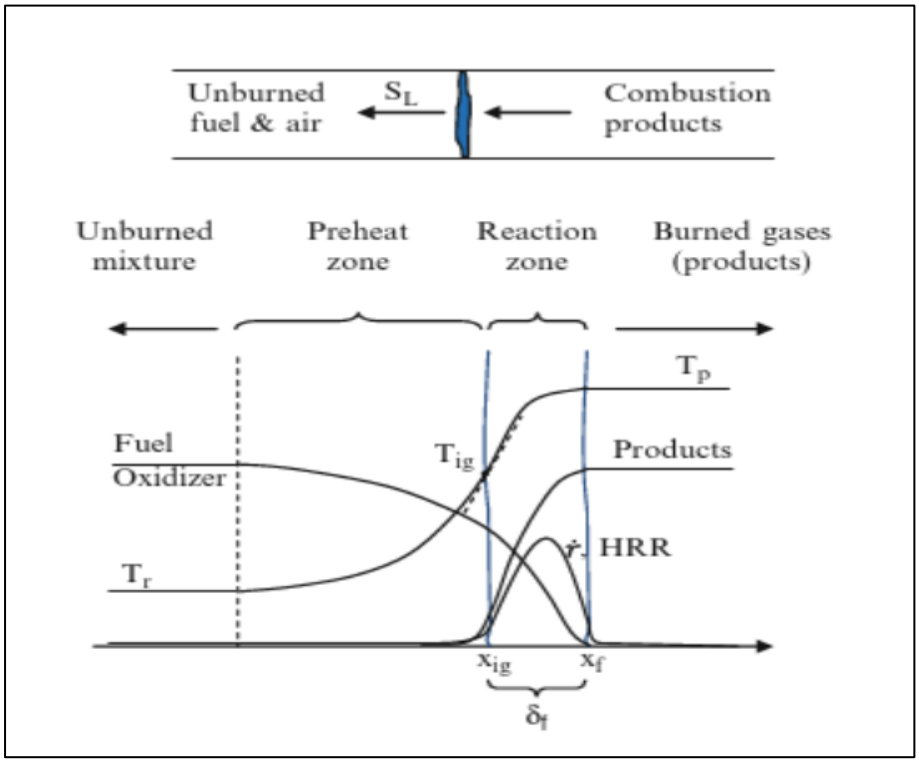

Figure 2.2: Premixed flame propagation in a duct [14]

The initial flame propagation is laminar, which propagates with laminar flame speed. Laminar flame propagation is happening due to two phenomena. Heat is transported to the unburned fuels and air through the preheat region, and combustion occurs at the flame. Thus, the flame speed depends on transport properties and reaction properties [14]. This propagation is usually subsonic. To sustain the flame, heat is released, and fuel is consumed. Equation 2.1 gives this consumption rate [15].

$$\dot{m} = \rho S_L A \tag{2.1}$$

$\dot{m}$ gives the rate of fuel consumption. ρ, S_L, A give the density of the gas, velocity of the gas, and area, respectively [15]. This was developed considering that unburned gases enter normal to the wave. The reaction depends on the area. However, this propagation can stop if flames hit a wall. It creates quenches, reduces the flame area, and affects the burning rates. This could create instabilities later during the flame propagation. The instabilities could cause wrinkles, which could generate turbulence and later influence the transition to detonation [13], [16].

2.1.2 Flame instabilities

Barrère and Williams [17] stated in their study that there are several combustion instabilities in a combustion chamber due to external or internal conditions. Internal conditions for instabilities are inherent to the reactants. External instabilities are acoustic instabilities due to acoustic waves, shock instabilities due to shock or detonation waves, and fluid dynamic instabilities due to flow patterns. Vortices are an example of such flow patterns.

Below are five instability mechanisms for premixed combustion: diffusive–thermal, Landau–Darrieus, Rayleigh–Taylor, Richtmyer–Meshkov, and Kelvin–Helmholtz.

2.1.2.1 Diffusive-thermal instability

This instability occurs in laminar flame propagation due to heat conduction or thermal diffusivity and chemical reaction or molecular diffusivity. This phenomenon could affect the reaction zone either to stabilize or destabilize. This instability can be explained using the Lewis number.

$$Le = \frac{\alpha}{D} = \frac{\lambda}{D \cdot \rho \cdot C_p} \tag{2.2}$$

In Equation 2.2, α is the thermal diffusivity, D is the molecular diffusivity and ρ, C_p, λ are density, specific heat, and heat conductivity, respectively. Depending on the Lewis number, the stability and instability of the flame can be identified. If $Le = 1$ then, flame is stable by increasing thermal diffusion and balanced by increasing heat loss due to molecular diffusion; thus, flame temperature and burning velocity don't change. If $Le > 1$ then thermal diffusion is greater than heat loss due to molecular diffusion, thus decreasing flame temperature and burning velocity. If $Le < 1$ then diffusion of molecules is higher, and both burning velocity and flame temperature will be increased, and it will increase the instabilities [13], [18].

2.1.2.2 Landau – Darrieus instability

This hydrodynamic instability occurs due to the interaction between a burnt product and an unburnt mixture in the reaction zone or density jump across the flame. This instability occurs in the velocity gradient across the flame front. The flame surface has perturbed, and velocities normal to the flame surface in burned and unburned sides adjacent to the flame surface are different. However, the tangential component of the velocity is continuing. Thus, streamlines converge and diverge at convex and concave areas of the flame, as shown in Figure 2.3. Due to this, the flame will increase the curvature. Hence, increased velocities and decreased velocities at local sections can be observed that amplify the flame wrinkling [13], [18].

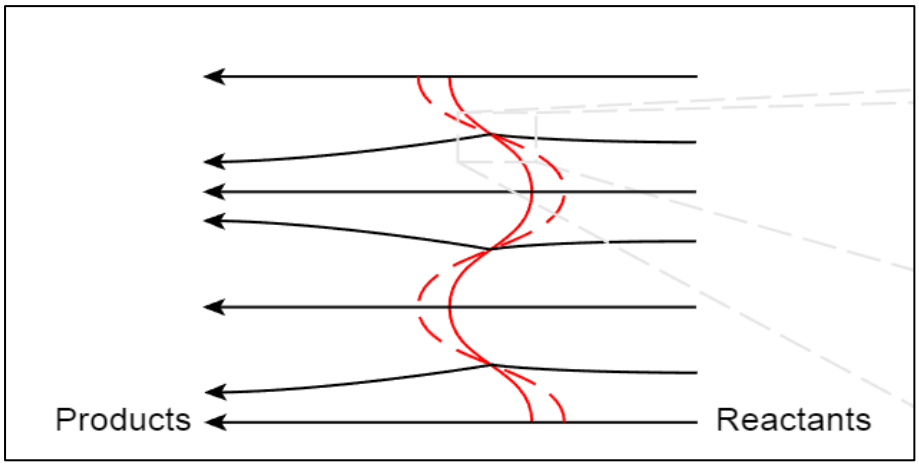

Figure 2.3: Mechanism of the Landau-Darrieus instability [19]

2.1.2.3 Rayleigh – Taylor instability

This is also a hydrodynamic instability, and it occurs during flame propagation of fluids with different densities due to body forces such as gravity. This instability can be called buoyancy-driven instability. Depending on the acceleration of the fluid type, this phenomenon can be stable or unstable. If lighter fluid accelerates toward the heavier fluid, then there will be instabilities. It can happen when unburnt gas is over the burnt gas since, typically, unburnt gas is denser than burnt products. This leads to the formation of finger-like structures that evolve into mushroom caps. This influences the flame speed, flame shape, and propagation characteristics and is thus called instability. However, heavier fluid accelerated towards the lighter fluid is considered stable [13], [18]. Figure 2.4

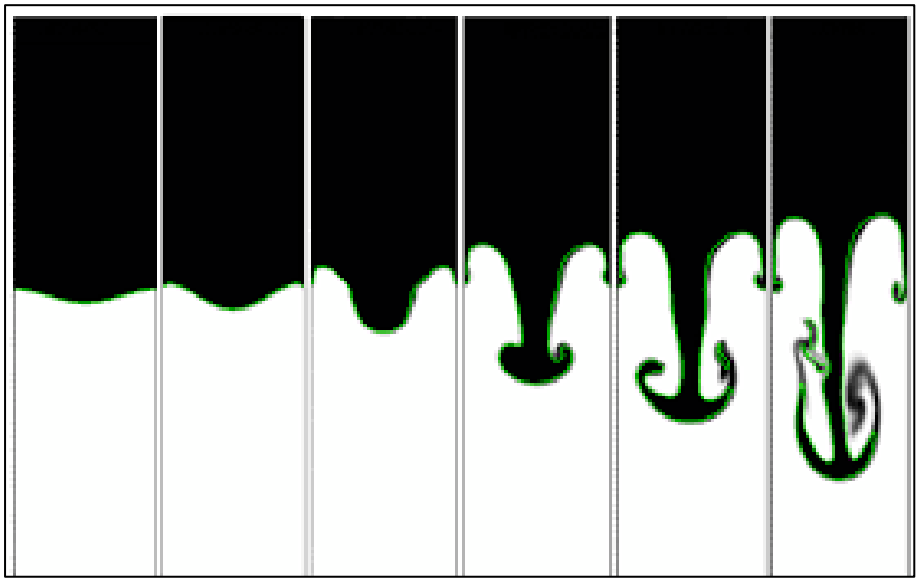

Figure 2.4: Illustration of Rayleigh-Taylor instability [20]

2.1.2.4 Richtmyer – Meshkov instability

This instability has similarities to Rayleigh-Taylor instability; however, it occurs due to impulsive acceleration, mainly due to shock waves. This instability occurs due to density difference, the same as Rayleigh-Taylor instability, but it is due to impulsive acceleration. So, this instability occurs in both the acceleration of lighter fluid in heavy fluid and the acceleration of heavy fluid in lighter fluids [13].

2.1.2.5 Kelvin – Helmholtz instability

This instability is also a hydrodynamic instability that influences flame dynamics and flame propagation. The surface of non-mixable, incompressible, and parallel-flowing fluids with different velocities could show this instability. It could create perturbations due to the shear forces, which are created by differences in the velocities of the two fluids [13].

2.1.3 Turbulent flame propagation

2.1.3.1 Turbulent flame

As shown in Figure 2.1, turbulent flames are the next evolution of flame propagation after the instabilities of the laminar flame. Turbulent flame propagation may drive the deflagration to detonation transition.

Kuo [21] says in his book that giving a precise definition of turbulence is a difficult task; however, it can be described using the characteristics of turbulence. Irregularity, diffusivity, Reynolds number, three-dimensional vorticity fluctuations, dissipation, continuum, and flow are the characteristics used in the book. Turbulent flows are irregular; thus, statistical methods are suitable for analyzing turbulence. The diffusivity of turbulent flows is high; therefore, rapid mixing increases heat, mass, and momentum transfer rates. Reynolds numbers are high in turbulent flows. Turbulence is three-dimensional and highly rotational; thus, changing vorticities are characteristic of turbulence, which is used to describe it. Turbulence flows are dissipative because they use kinetic energy to work against viscous losses. Turbulence is a flow of fluid and a continuum phenomenon.

Turbulent-premixed flames propagate faster than laminar-premixed flames, and eddy diffusivities are one of the reasons [14]. Interaction between the flame and premixed gas flow depends on the length and time scales for gas flow and flame. Borghi diagrams can summarize turbulent premixed combustion.

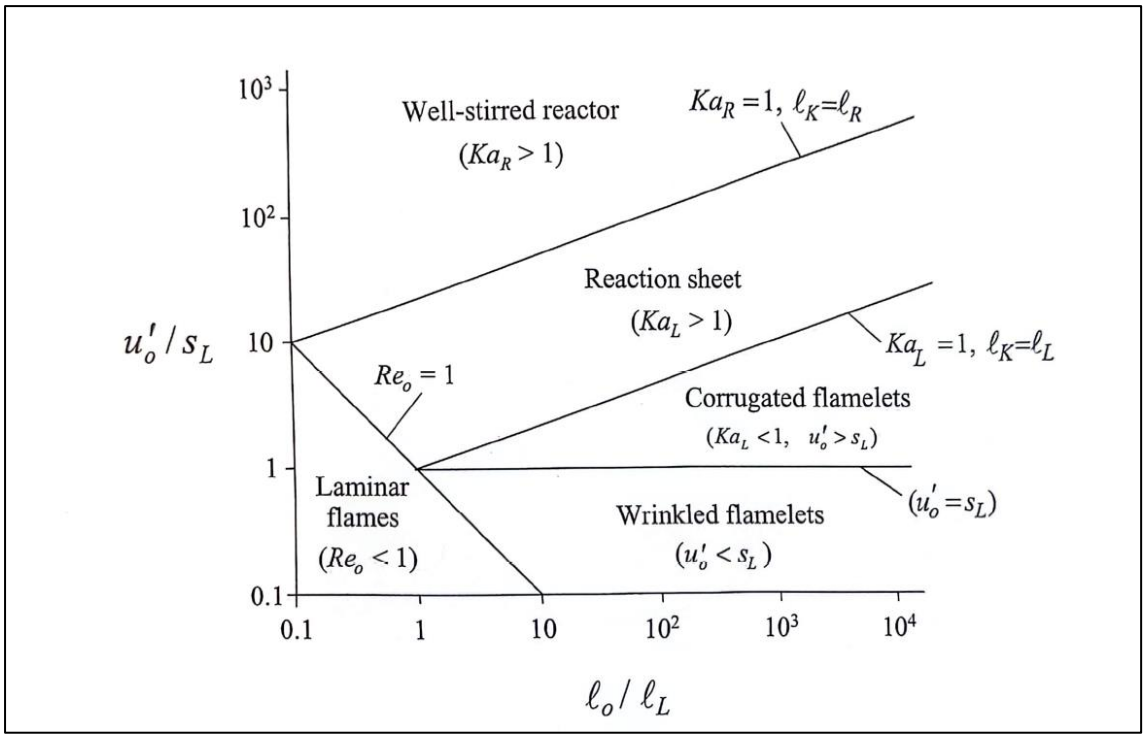

Figure 2.5: Diagram of premixed turbulent combustion regimes [18]

The line where Re_0 is equal to one separates the laminar and turbulent regions. Turbulent regions can be separated into four regimes, as shown in Figure 2.5. The region where turbulent intensity (u_o') is smaller than laminar burning velocity (S_L) has a flame that is only wrinkled, and this shows that turbulence is slower than the advancement of the flame. Even though this is in the turbulent flow field, the flame keeps its laminar structure. However, the flamelet surface is slightly wrinkled when passing the eddies [13], [18].

The corrugated flame-let region's turbulent intensity is greater than the laminar burning velocity, and the flame is highly twisted during traveling due to eddies. This will make a part of the flame front connect with another part of the flame front to create pockets of burned or unburned mixtures. However, the structure of the flame element remains laminar [13], [18].

In the reaction sheet region, the flame behaves as a flame-let, and the flame front is not laminar. Small eddies penetrate the preheat zone, increasing the region's heat and mass transfer rates. So, the flame is expanding. The reaction sheet only wrinkles, and the structure doesn't get affected by eddy motion [18].

The last region acts as a well-stirred rector in combustion reactions. Heat diffusion to the preheat zone can be observed. Eddies penetrate the reaction zone structure, creating diffusion and heat transfer to the pre-heat zone. This could cause a temperature drop in the flame and eventual extinction of the flame [18].

Turbulence flames are normally combined with noise and changes to the flame envelope. Since turbulent flames are described using the equations for flow properties, they are not as well defined as laminar flames [21]. Turbulence affects the flame in many different ways; eddies are one of them. Eddies are characterized by average rotational velocity and length scale. The characteristic length is called the integral length scale, which Equation 2.3 defines.

$$l_0(x,t) = \int_0^{\infty} f(x,r,t) \tag{2.3}$$

Where $l_0(x,t)$ is the integral length scale of an eddy at x distance from a reference point at a given time while $f(x,r,t)$ is the normalized correlation function for eddies considering cartesian coordinates. The smallest turbulent scale is the Kolmogorov scale. These two length scales are used to define turbulent flows.

Knudsen [13], reviewed several other studies to summarize the effect of turbulence combustion regimes and turbulent flame propagation in pipes toward DDT. In this review, turbulent flame propagation is divided into three combustion regimes. They are the subsonic combustion regime, the choked combustion regime, and the quenching regime. The study summarizes that Dorofeev et al. [22] observed three different regimes through the experimental results, and they are subsonic and choked combustion regimes, quenching of the flame, and quasi-detonations. Total quenching of hydrogen and air flames is not always possible, but due to the unpredictability of turbulence, changing combustion regimes is possible. After evolving to turbulence, the flame could transition into detonation, as shown in Figure 2.1.

2.2 Detonation

Detonation is combustion with supersonic flame propagation relative to the unburnt gas. It is considered as the most devastating form of gas explosion [23]. Gas explosions are not always detonations. However, they start as deflagrations, which are explained in previous sub-chapters, and they are traveling subsonic velocities reference to the unburnt gas velocities. These deflagrations can transition into detonations that are supersonic. When deflagrations propagate, they send pressure waves and sound ahead of the flame or the reaction front, which can be used to identify this ahead of the flame front. However, detonations do not send such information when propagating [8]. When a combustion reaction occurs behind a shockwave, the shock wave compresses the unburnt gas and heats up to auto-ignition temperature. This causes the premixed gas to auto-ignite and release heat rapidly, which expands the gas and supports the shock wave to propagate. This complementing phenomenon makes detonation self-sustaining and propagating at supersonic conditions [13].

Chapman-Jouguet theory (CJ theory) is a one-dimensional consideration. The conservation of mass, momentum, and energy is considered in this analysis to derive a unique solution to detonation velocity. The detonation velocity and pressure can be calculated for a known gas mixture using the CJ theory without chemical reaction rates [23]. CJ detonation velocities and pressures for the hydrogen-air mixtures with initial conditions at 25 ^{o}C and 1 atm pressure are 1968 ms^{-1} and 15.8 bar, respectively [23].

Zel'dovich, von Neumann, and Döring (ZND) suggest different propagation methods and structures for detonation waves. This suggests an infinitely thin shock wave that leads to the detonation front. This shock wave compresses the reactants to high pressure and high temperature, which keeps the leading shock at constant energy by auto-igniting. So, the detonation is propagated by the leading shock wave, and behind the shockwave, there is an induction zone where the pressure, temperature, and density profiles are flat. Behind the induction zone, the reactant will drastically change properties by reacting. This zone is the

reaction zone. This structure is a more detailed structure of detonation than explained by CJ's theory. The structure and the property changes are shown in Figure 2.6 [21].

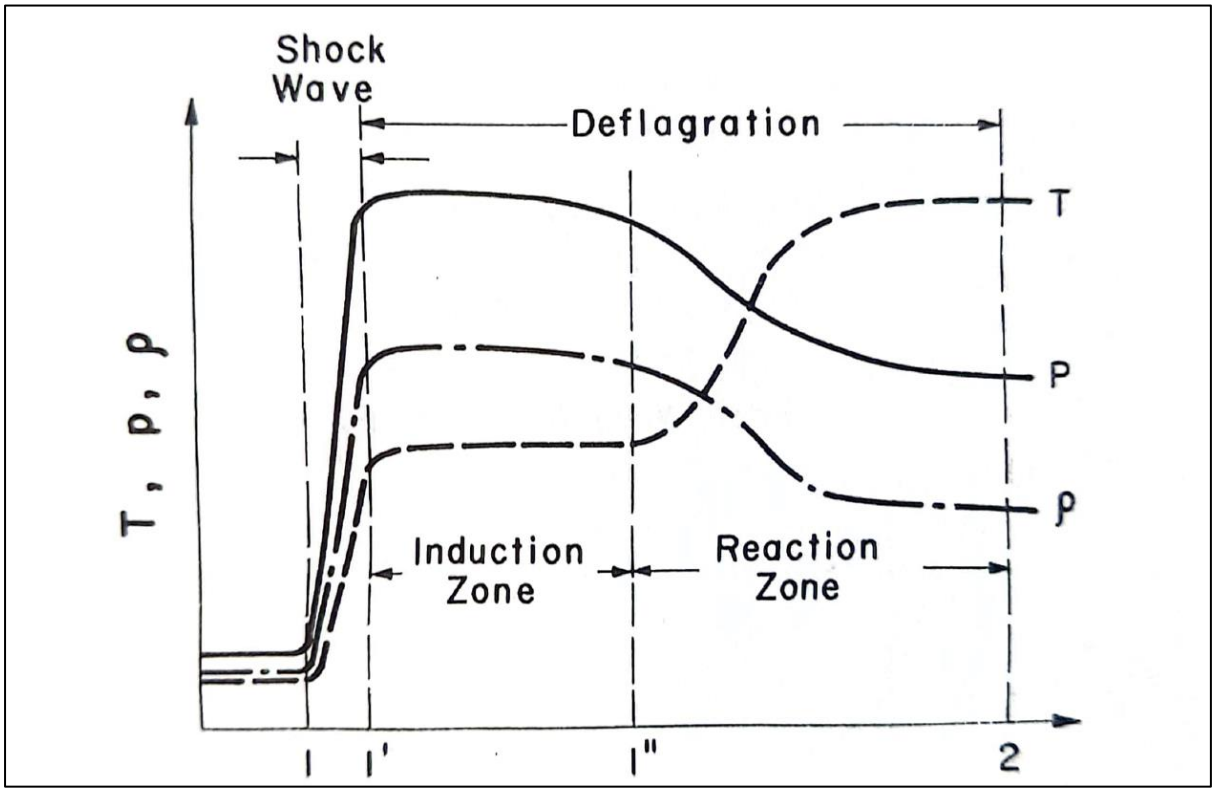

Figure 2.6: Change of physical properties of s ZND detonation wave [21]

Both above theories use one-dimensional analysis, but detonation is a three-dimensional phenomenon. The detonation wave structure characterized by multidimensional leading shock waves shows many curved shockwaves. These curved shock waves have intersections propagating in different directions with high velocities. The intersections of these waves are called triple points, and these triple points make cell-type structures. The length scale of these cells is used as a characteristic value to talk about detonability. The cell size is approximated value, and larger cell sizes show higher resistance towards detonation [21]. Small cell sizes in hydrogen and air mixtures make detonability high in hydrogen-air-premixed explosions [23]. The cell structure of a detonation is shown in Figure 2.7.

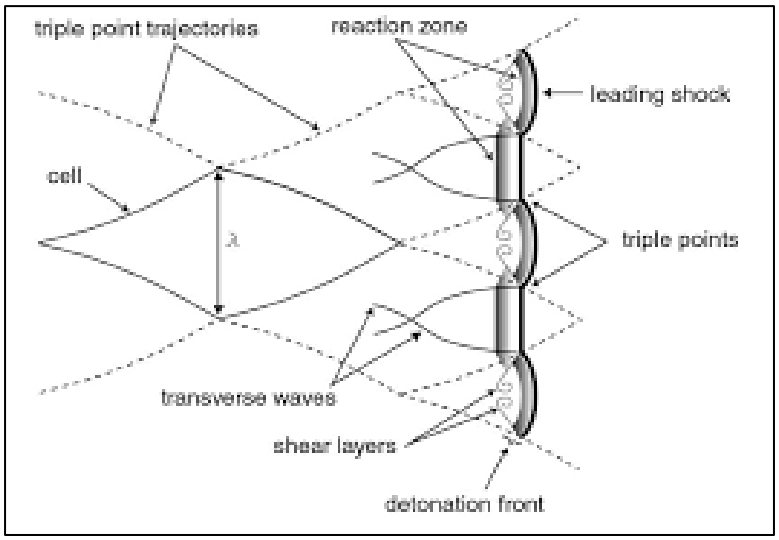

Figure 2.7: Sketch of triple point and detonation cell structure [24]

2.3 Deflagration to detonation transition (DDT)

2.3.1 Deflagration to detonation transition (DDT)

DDT is considered a phenomenon with no clear explanation. Quantitative prediction of DDT is difficult since it requires much information, such as the dynamics of interactions among flames, shocks, boundary layers, and turbulence [25]. Knudsen's study [13] mentions two methods that can make the transition to detonation. The first method is the leading shock wave, creating an autoignition in unburned gas. The occurrence of this should fulfill two scenarios. The first requirement is that energy should be released into unburned gas, and that amount should be like creating a shock wave in CJ detonations. The second requirement is that the time scale of the created shock wave be greater than or equal to the induction time [13], [16], [25], [26]. The second method is due to flame stabilities and mixing. The combined effects of pockets of unburned gases, confinement, and shockwaves cause this [13].

Kuo's book [21] explains the development of detonation using several steps. They are the generation of compression waves, the formation of shock, the movement of gases due to shock and breaking the flame into the turbulent brush, explosions within the turbulent reaction zone and the occurrence of transverse waves and retonation, the development of spherical shock waves, the interaction of transverse waves with the shock front, retonation wave, and reaction zone, and the formation of the steady wave, which is self-sustaining CJ detonation.

Chung K. Law wrote in his book "Combustion Physics,"

"Conceptually, the problem of DDT consists of describing the physical processes that are responsible for the acceleration of a flame, propagating via mass and heat transport at velocities lower than a few meters per second." [18]

Law [18], in his book, says that in this transition, diffusive transport of molecules gets dominated by convective transport and ignition influenced by shock compression. So, DDT studies should consider how waves change from diffusive to convective. Considering a smooth tube, initially, flame diffusion dominated during flame propagation. However, due to the

expansion of burned gas, a compression wave is generated ahead of the flame. Generated compression waves will combine and form a shock that increases the pressure and temperature of the unburnt gas. This leading shock changes the conditions of unburnt gas, reducing the induction delay. Due to this phenomenon, spontaneous fast flames develop by replacing the diffusive quality of the flame with convective qualities. This acceleration creates detonation waves and transitions into detonation [18].

2.3.2 Experimental studies of explosions in channels on DDT

Gas explosion and DDT studies are conducted using channels on a laboratory scale to understand the phenomenon. Understanding this helps to improve process safety measures and reduce consequences.

Kuo states in his book, using the experimental study of Urtiew and Oppenheim [21], [27] which was conducted inside a one-meter tube for hydrogen and oxygen mixtures; detonations occur in different areas of the flame propagation. Depending on the location, the study identifies four modes of detonations: detonation between flame and shock front, at flame front, at shock front, and at contact discontinuity. This is shown in Figure 2.8.

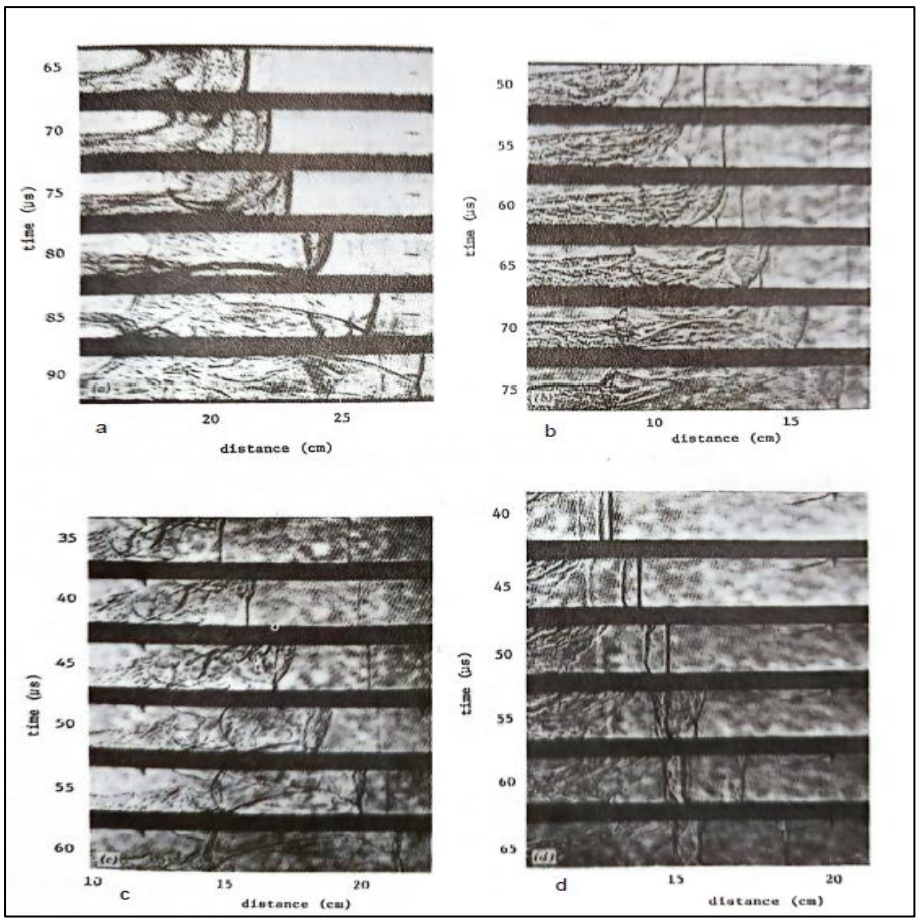

Figure 2.8: Various transition to detonation modes observed in $2H_2 + O_2$ mixtures by Urtview and Oppenheim [21], [27]. (a) detonation occurring between flame and shock, (b) detonation occurring at flame front, (c) detonation occurring at shock front, (d) detonation occurring at contact discontinuity

Knudsen [13] has conducted gas explosion experiments for various fuels and air mixtures with different equivalence ratios inside single obstructed closed circular pipes in multiple lengths. The primary objective of the study was to analyze the effects of blockage ratio and equivalence ratio on flame propagation. The experiment was done at atmospheric pressure and temperature for three pipe lengths of 3, 4, and 7 meters, and the 4-meter and 7-meter pipes had obstacles. The experiment was done for four types of fuels. They were hydrogen, hydrogen and carbon monoxide mixture, propane, and methane. Detonations were observed in both hydrogen-air mixture and hydrogen, carbon monoxide, and air mixture during the experiments. However, DDT was not observed in the methane and propane mixtures during the experiments. The results of these experiments conclude that detonations occurred for blockage ratios ranging from 0.572 to 0.965 for the four-meter pipe. This happened with hydrogen and air mixture at equivalence ratios from 0.79 to 1.95. This corresponds to obstacle opening diameter ranging from 70 to 20 mm and hydrogen volume percentage ranging from 25% to 45%. The study has concluded that most ideal conditions for DDT occurred with a blockage ratio of 0.921. Further, the cell size, the pipe diameter, and the obstacle opening diameter were identified as important parameters for DDT in an obstructed pipe. However, experiments in a four-meter pipe revealed that the distance between the pipe end and the obstacle opening is also a critical length scale. Experiments with carbon monoxide, hydrogen, and air at stoichiometric levels revealed that adding small amounts of carbon monoxide to a hydrogen-air mixture did not affect the detonation properties of hydrogen. DDT was observed in this mixture at a hydrogen volume percentage of 27. Propane and methane mixed with air at stoichiometric conditions have shown an intriguing discovery where pressure recording shows that flame was extinguished at the blockage ratio reached 0.991 [13].

Gaathaug [8] has conducted a study focusing on DDT and flame propagation before obstacles. During the study, hydrogen-air homogenous and inhomogeneous mixtures were exploded in 100 mm X 100 mm square transparent channels, which had 1500mm and 3000mm lengths. Experiments were conducted for different blockage ratios. The blockage ratio was changed by changing the opening in the middle of the channel. High-speed imaging and Schlieren techniques were used for the analysis. The study discusses homogeneous mixture explosion results, concluding that blockage ratio plays a crucial role in determining the intensity of the jet formed after the obstacle and turbulent burning. When the blockage ratio is too small, the turbulence intensity is insufficient, leading to the absence of DDT. Additionally, the reactivity of the mixture is a significant factor, with DDT not being observed for mixtures containing less than 28% hydrogen in the air. The highspeed image data obtained during this study showed powerful transverse waves in the channel before the detonation. Detonations were mostly observed on the top wall; however, two detonations were observed on the bottom wall. Highspeed image data observed a spot of bright light, which is identified here as DDT or local explosion. The study concluded that local explosions were observed due to transverse waves, which initiated and amplified other local explosions, leading to detonation. The study concludes by comparing with Knudsen's study [13] that it is reasonable to assume that DDT occurs at walls of circular pipes as well. The study discusses the results obtained by inhomogeneous mixture explosions, which were similar to homogeneous mixture explosions since they mirrored the same events during DDT. It also adhered to the same concentration limit of 27% hydrogen in the air, and the flame burned rapidly after the obstacle, causing local explosions and transverse waves that created detonations. The study concluded by showing that introducing air into the channel before ignition to make it an inhomogeneous mixture did not affect the DDT [8].

Henricksen et al. [9], [10] investigated the random nature of the DDT for hydrogen and air mixture in a one-meter-long explosion channel. The same channel is used in the current study. DDT occurred in 10 of the 20 experiments conducted under identical initial conditions and a fuel-air equivalence ratio 1.2, indicating the probability of DDT of 50% in this setup. The study observed 78 % and 80% DDT in experiments done for the equivalence ratios 1.0 and 1.1, respectively. Highspeed images revealed that hotspots were formed slightly downstream of the obstacles during DDT. A hypothesis was suggested from this study that the collision of two opposing transverse pressure waves leads to the formation of this hotspot. The pressure waves result from local explosions of the flame exiting the top and bottom of the obstacles. The study didn't see any hotspots in the experiments where DDT didn't occur. The study further discusses that quenching and re-initiating could occur inside the obstacles since the gap between obstacles is smaller than the detonation cell size. It was mentioned in the study that a hot spot was always observed in the center of the channel close to the end of obstacles. When DDT occurred, the hot spot was transported toward the upper or lower wall with flame propagation, and DDT occurred at the wall [9].

3 Experiments

DDT of hydrogen-air gas explosions in a one-meter channel has been studied for this report. The background of this experiment was motivated by the studies done by Henriksen, Gaathaug, Vågsætheer, and Bjerketvedt. Henriksen et al. [9], [10] had done a study on DDT in a one-meter channel with circular obstacles. The setup for this study is the same as the experiments done by Henriksen et al. [9], [10]. The background of the experiments was to study hotspot and DDT further. Henriksen et al. [9], [10], [11], [12] explained this experimental procedure in several publications, which is explained here to give the reader a perspective of the experiments.

3.1 Experimental setup

This section gives an overview of the experimental equipment, data acquisition, and data post-processing used in this study.

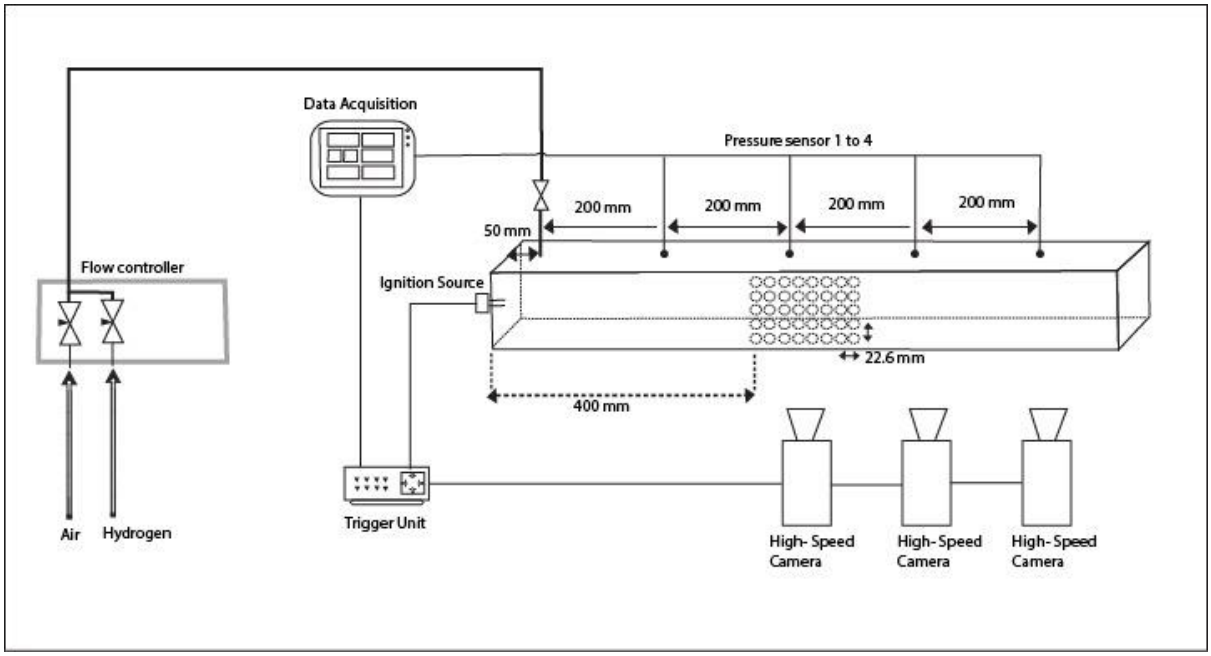

Figure 3.1: Schematic illustration of the experimental setup [10].

Explosion channel

The experiments were done in a 1-meter-long rectangular open-ended channel, shown in Figure 3.2. The height and the width were 116.5 mm and 65 mm respectively. The premixed gas inlet was positioned at the top of the channel, 50 mm from the back end. A pneumatic on/off valve controls the flow. A porous lid was installed at the open end of the channel to prevent gravity currents and to ensure that the concentration inside the channel was homogeneous. This porous lid was released just before ignition. A spark plug was installed at the back end of the channel for ignition. The ignition source was a 230 V AC transformer with an output voltage of 10 kV RMS to generate the high voltage spark. Explosion pressure was measured using four Kistler 7001 pressure transducers installed on the top wall of the channel. The first transducer was positioned 250 mm from the back end of the channel. The rest of the transducers were

positioned with equal intervals of 200mm. There were 40 obstacles placed inside the channel, 400mm from the back end. These obstacles are identical and have the size of an 18650-battery cell, which is 18 mm in diameter and 65 mm in height, and the gap between the two obstacles is 4.6 mm. The maximum blockage ratio is 0.77, and the void ratio is around 0.5.

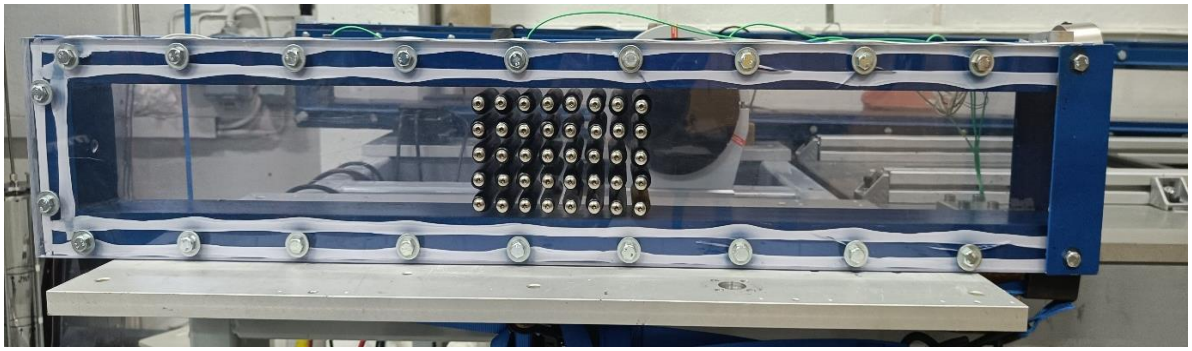

Figure 3.2: Explosion channel used in this experiment

Gas handling unit

The gas handling unit was used to send homogeneous hydrogen and air mixture to the explosion channel. The compressed air was produced by an oil-free air compressor, and commercial-grade hydrogen was provided using a high-pressure hydrogen cylinder. Correct mass flows for air and hydrogen for the desired equivalence ratios were calculated beforehand using Cantera. These flows were measured and regulated using low-flow Coriolis mass flow meters given to a single gas supply line and sent to the explosion channel for a premixed homogeneous hydrogen-air mixture.

Data acquisition

The data acquisition system consists of several items: a pressure data acquisition system, a mass flow data acquisition system, a high-speed camera system, and a trigger unit combined with an ignition box. The ignition box initiated the trigger signal for the entire data acquisition except mass flow data acquisition. The high-speed camera system had three cameras: Photron SA1, Photron SA-Z, and Kirana 5M. SA-1 operated with 8000-10000 frames per second speed, SA-Z operated at 120000 frames per second speed, and Kirana 5M operated at 400000-500000 frames per second speed. High-speed images were saved and processed later using Python. Pressure data was generated from the four transducers and was recorded using a laboratory computer to process it later. Mass flow data was recorded in a separate oscilloscope, extracted, and stored for post-processing.

Data post-processing

All the different data acquired during one explosion experiment were post-processed using Python. The codes for this were provided. They were used previously by Henriksen et al. [9], [10], [11] . Some of the improved codes for image processing developed by Peter Bosnic is used to process data. The highspeed camera images of SA-1 and SA-Z, pressure data, and mass flow data were processed using the provided codes to analyze flame positions, flame speeds, and pressure inside the channel.

Flame front velocities calculated from raw flame tracking data were filtered using the Savitzky-Golay filter [28] with second-order central differencing to smoothening. The window length

was defined considering the number of data points. The same filter was used by Henriksen et al. [11], [12] to analyze the same type of data.

Changes in experimental setup from previous studies

The current setup only has one major difference: the automatic ignition box. This ignition box was provided to improve the previous procedure and automate the ignition and lid dropping. The ignition box takes 20 seconds of preparation time to give the trigger signal to the system. The lid dropping and trigger signal had a gap of 1 second. These times were decided based on the previous study and results.

3.2 Experimental procedure

All the experiments were done in the same manner but on different days. On average, around 7 to 10 experiments were conducted using the setup mentioned above, and the procedure for each experiment was as follows.

Pre-preparation was done before the start of the experiment procedure to ensure the experimental results' repetitiveness. First, the safety of the rig and the area was secured, and then the camera system was calibrated. Each day after calibration, a picture of the experimental setup was captured to get the necessary data to feed the camera data post-processing code.

The experiment started by flushing the channel for 300 seconds (about 5 minutes). After flushing was stopped, waited until the flow meters reached 0 and the mass flow data acquisition system was started. At the same time, the channel was closed using the porous lid and kept for 30 seconds to develop a baseline for mass flow data. After 30 seconds, the filling was started according to the intended equivalence ratio values. The mass flow meters were adjusted using manual valves to achieve desired flow rates. The filling was done for 300 seconds (about 5 minutes) to ensure the channel was homogeneous. After this, within the next 60 seconds, data acquisition systems for pressure and highspeed images were reset and readied for the trigger, and mass flow data acquisition was stopped. After that, the automatic trigger button was pressed, and after 20 seconds, it sent the trigger signal for the ignition and the data acquisition system to start. Then, the highspeed image, pressure, and mass flow data were stored. In the end, channel flushing was started again to prepare for the next experiment. Experiments were done in the steps mentioned above; they can be considered similar and repetitive.

3.3 Experimental matrix

During the experimental stage of the study, 112 experiments were conducted, and the full experimental details are shown in Appendix B. The summary of these experiments is shown in Table 3.1. The 112 experiments were conducted as seven projects. These details are available in Appendix B and Table 3.2.

Table 3.1: Experimental matrix.

Equivalence ratio	Experiments	No ignitions	Post-processing errors	DDTs	Experiments after the repair
0.8	9	-	1	-	2
0.9	10	-	2	-	2
1.0	10	-	1	-	2
1.1	40	1	2	6	14
1.2	8	-	1	-	1
1.3	9	-	-	-	2
1.4	10	-	2	-	2
1.5	9	-	1	-	2
1.6	7	-	-	-	1
Total	**112**	**1**	**10**	**6**	**28**

Out of all experiments, 11 were not considered in further analysis due to post-processing errors and one incident of not observing the ignition. Only six detonations were observed from 112 experiments. During the experimental study, a leak from the explosion channel was observed and repaired by changing the gaskets. After the repair, 28 explosion experiments were conducted. The experimental study was conducted through seven projects. Each project was created due to a major change to the process rig or a major change to the objective. The distribution of experiments of the projects is shown in Table 3.2.

Table 3.2: Tabel for details on experiments (project number-based)

Project name	Experiments	Equivalence ratio								
		0.8	**0.9**	**1.0**	**1.1**	**1.2**	**1.3**	**1.4**	**1.5**	**1.6**
P101	7	0	1	1	3	1	-	1	-	-
P102	36	4	4	4	4	4	4	4	4	4
P103	8	1	1	1	5	-	-	-	-	-
P104	23	2	2	2	4	2	3	3	3	2
P105	10	-	-	-	10	-	-	-	-	-
P106	4	-	-	-	4	-	-	-	-	-
P107	24	2	2	2	10	1	2	2	2	1

Total	**112**	**9**	**10**	**10**	**40**	**8**	**9**	**10**	**9**	**7**

Projects P106 and P107 were conducted after the repair and rest before observing the leak. After the repair, a concentration test was conducted without ignition to ensure the channel was not leaking. The same experimental procedure was followed to understand the concentration profile during filling; however, it was done by disconnecting the ignition source. During the concentration check, four sensors were used. All of them were between the end of obstacles and the open end. Gathered data was used to check that concentration anomalies occur due to leaks. However, this test revealed that there aren't any leaks, and the concentration profile is homogeneous. This will be discussed further in the next two chapters.

4 Results and discussion

The results obtained from the study are shown and discussed in this chapter. The results are based on pressure, mass flow, and image data. The results are presented by separating data obtained before and after the repair of the channel. Post-processed results obtained from 101 experiments were separated according to the intended equivalence ratio. From them, an error of 0.035 on negative and positive to the equivalence ratio was considered to separate experimental results to present this chapter. The details of the number of experiments used in the analysis are mentioned in Table 4.1. The pressure sensor data analysis is based on the experiments mentioned in Table 4.1. Further details on these experiments can be found in Appendix B, C, and D. Other than these, all image and pressure data of DDT have been used to examine the phenomenon.

Table 4.1: Table for details on the number of experiments used for the data analysis.

Equivalence ratio	**Experiments within ±0.035 error**	**DDTs**	**Experiments after the repair**
0.8	4	-	2
0.9	3	-	2
1.0	5	-	2
1.1	27	5	13
1.2	3	-	1
1.3	2	-	-
1.4	4	-	1
1.5	3	-	2
1.6	2	-	-
Total	**53**	**5**	**23**

4.1 Pressure and highspeed image data analysis

4.1.1 Pressure data analysis

Peak pressure is a significant data point in this study. Trends of the peak pressures for different equivalence ratios provide important information on the energy released in gas explosions. Table 4.2 shows the maximum, minimum, and mean peak pressure values obtained from the raw pressure data. For every pressure sensor, the highest maximum peak pressures and highest

mean peak pressures were observed between the equivalence ratios of 1.0 and 1.2. Most of the DDT observed by Henriksen et al. [9], [11], Gaathaug [8], and Knudsen [13] were in similar equivalence ratios. The highest peak pressures are likely to be observed in that region, with the highest tendency to observe DDT. This trend shows that experiments were trending in the expected direction, and it was the same as previous studies, even though the observed DDT cases were low.

On average, the highest peak pressures were observed in pressure sensor four, and the peak pressure at pressure sensor four was always higher than at pressure sensor three. This is observed in experiments where both deflagration and detonation occurred, and it is also observed before and after the repair. However, Henriksen et al. [9] observed the highest mean peak pressure at pressure sensor three for deflagrations. This is a difference observed during this study compared to the previous studies on this channel.

Higher peak pressures were observed at pressure sensor two compared to pressure sensor three; this could be due to the chaotic nature of the flame propagation through the obstacle array. Local explosions inside this array could create these pressure peaks. However, there are cases where the opposite was observed. The pressure variation at pressure sensor two during turbulent flame propagation is chaotic, so it is hard to explain the exact reason for this observation. Henriksen et al. [9] explained that there was a possibility of quasi-detonations inside the obstacle array during flame propagation. However, it is hard to determine the occurrence of quasi-detonations using the Schlieren images or highspeed images. The gap between any two obstacles is 4.76 mm, and this is below detonation cell sizes for the hydrogen-air mixtures [23]. Detonation could not propagate within this array, and the higher peak pressures observed at pressure sensor two could be quasi-detonations.

Table 4.2: Peak pressure analysis for deflagration and detonation experiments

Deflagrations												
Phi	**PS1 [bar]**			**PS2 [bar]**			**PS3 [bar]**			**PS4 [bar]**		
	Max	**Min**	**Average**	**Max**	**Min**	**Average**	**Max**	**Min**	**Average**	**Max**	**Min**	**Average**
0.8	3.2	2.1	2.6	10.3	3.7	6.0	4.6	2.8	3.9	6.3	4.0	5.0
0.9	2.8	2.5	2.6	9.1	4.9	7.2	4.9	3.8	4.2	8.3	6.0	7.2
1.0	3.0	2.5	2.8	9.3	5.5	7.1	6.0	3.3	5.0	11.0	6.5	8.4
1.1	4.4	2.6	3.2	12.3	5.0	7.0	6.7	3.3	4.5	11.1	5.5	8.6
1.2	3.5	2.9	3.3	9.4	4.7	7.7	5.6	3.7	4.6	8.6	6.4	7.4
1.3	3.2	2.8	3.0	8.0	6.2	7.1	4.4	3.5	3.9	8.6	8.1	8.4
1.4	3.1	2.7	2.9	7.7	4.8	5.8	4.8	2.9	3.6	7.4	5.5	6.8
1.5	3.1	2.6	2.9	7.5	5.1	6.5	6.8	2.7	4.9	5.9	4.4	5.3
1.6	3.1	2.7	2.9	5.0	4.8	4.9	2.9	2.6	2.8	5.7	4.8	5.2
Detonations												

Phi	PS1 [bar]			PS2 [bar]			PS3 [bar]			PS4 [bar]		
	Max	Min	Average	Max	Min	Average	Max	Min	Average	Max	Min	Average
1.1	4.6	3.5	4.0	17.3	5.4	10.2	10.5	6.7	8.7	37.7	17.7	23.4

However, detonations were only observed in very few cases. Even though the peak pressures showed a similar trend as previous studies, detonations did not occur as expected. DDT was only observed on an equivalence ratio of 1.1 on six occasions with 40 experiments. Maximum, minimum, and mean peak pressures for the observed DDTs show higher values compared to the study by Henriksen et al.[9]. The same study shows similar mean peak pressures at pressure sensors three and four. However, the results here show significantly higher pressures at pressure sensor four. Since the detonations observed in this study are very low, it is extremely difficult to observe trends from pressure data.

A comparison of the deflagration peak pressures observed before and after the repair, as shown in Table 4.3, shows no significant difference. However, mean peak pressures for pressure sensors three and four increased slightly after the repair. However, no significant differences were observed before and after the repair to connect with the low occurrence of DDT.

Table 4.3: Peak pressure comparison for the experiments before and after the repair

Deflagrations												
Phi	PS1 [bar]			PS2 [bar]			PS3 [bar]			PS4 [bar]		
	Max	Min	Average	Max	Min	Average	Max	Min	Average	Max	Min	Average
Before repair												
0.8	3.2	2.8	3.0	10.3	4.6	7.4	4.3	2.8	3.6	6.3	5.2	5.7
1.0	3.0	2.8	2.9	9.3	5.5	7.3	5.6	3.3	4.5	11.0	6.5	8.3
1.1	4.4	3.0	3.3	12.3	5.0	7.9	5.5	3.3	4.0	11.1	5.5	8.4
After repair												
0.8	2.4	2.1	2.2	5.6	3.7	4.6	4.6	4.0	4.3	4.6	4.0	4.3
1.0	2.8	2.5	2.7	7.8	5.8	6.8	6.0	5.4	5.7	9.4	8.0	8.7
1.1	3.5	2.6	3.1	6.5	5.1	5.6	6.7	4.3	5.1	10.6	6.3	8.8

Pressure and image data generated from an experiment are necessary to study simultaneously to understand and explain some observations of the study. Figure 4.1 shows the pressure data recorded from the ignition point to the flame front reaching the channel opening, while Figure 4.2 shows the flame propagation results obtained from processed highspeed images. The initial overpressure before point B in Figure 4.1 for pressure sensor two shows the pressure inside the channel when the flame propagates before obstacles. After point B, the graph shows the flame propagation after hitting the obstacle array. A, B, C, and D, marked in Figure 4.1, represent

points of the first peak pressures for each pressure sensor. Each point represents the pressure waves or pressure waves coupled with turbulent flame reaching the pressure sensor for the first time. The pressure peaks observed by pressure sensors after the initial peak are due to reflections of the pressure waves from the walls and obstacles. Thus, the initial peak is important information in energy released by the propagating flame and the impulse the wave can create. Time and pressure are important in calculating impulse [23], but this study doesn't study impulse; thus, this will not be discussed further here.

To understand the raw pressure data recorded in this experiment, the pressure readings will be separated into two parts: pressure data during laminar flame propagation and turbulent flame propagation.

Figure 4.2 shows the processed image data for the two sections in the channel. Image 4.2-A shows the flame propagation inside the channel before the obstacles where the laminar flame propagation can be observed. From here onwards, this channel section will be known as channel section one. Image 4.2-B shows the flame propagation inside the channel through the obstacles where turbulence can be observed. From here on, this channel section will be known as channel section two.

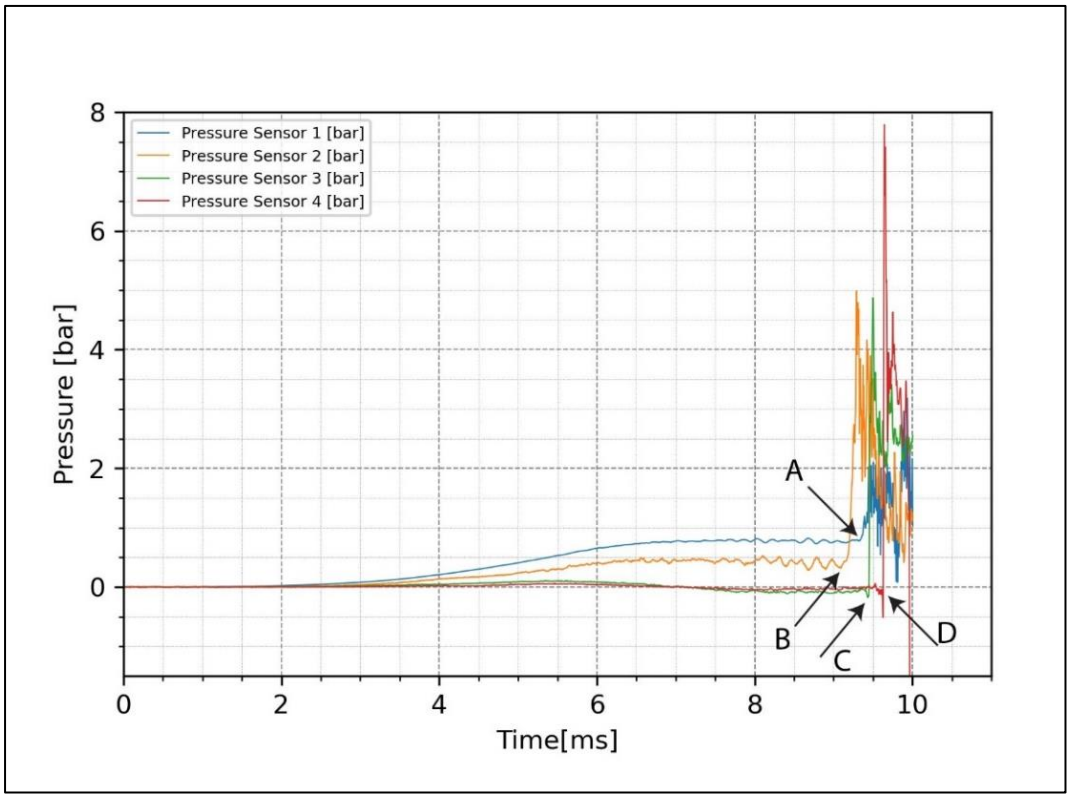

Figure 4.1: Pressure sensor readings of the explosion experiment P105_T00001 (the equivalence ratio is 1.1)

Flame propagation in channel section one is laminar. During this propagation, pressure sensors one and two show a continuous pressure increase due to the expansion of the unburnt fuel and burnt product. Due to the obstacles, the flow of unburnt fuel is hindered and trapped in the channel; thus, the pressure increase in sensor one and sensor two is observed. However, when

the flame reaches the obstacles, it transitions into a turbulent flame and propagates forward toward the opening of the channel. Pressure waves generated during the transition propagate in every direction by reflecting on obstacles.

The overpressure observed in channel section one is an important result since it creates the pressure difference required for the flow of unburnt gas inside the channel. The differences in this overpressure for different mixtures will be discussed later in this chapter to understand how it affects flame propagation.

The positions A, B, C, and D were used to distinguish the effects of turbulent flame propagation during the pressure data study. B, C, and D points are where the turbulent flame first reaches pressure sensors two, three, and four, respectively. Point A shows the pressure waves reflected from obstacles reaching pressure sensor one for the first time. The turbulent flame reaches the pressure sensor two first since it is the nearest to the start of the turbulent flame, shown in point B in Figure 4.1. When the reflected pressure waves reach pressure sensor one, the reading at pressure sensor one shows a sudden increase, as shown in point A in Figure 4.1. Point C shows the moment that turbulent flame reaches the pressure sensor three. Points A and C have similar times, but A is observed before C since the traveling distance to pressure sensor three is higher than one. Point D shows when the turbulent flame reaches the pressure sensor four. These points can be correlated with the times shown in Figure 4.2.

Combining these two data types could help understand the pressure data and how it changes with each phenomenon inside the channel. Separating and analyzing these two channel sections would provide a better understanding of the experimental study and the DDT phenomenon. The separation of pressure data is based on the pressure rise of pressure sensor two, which receives the effects of turbulence flame first. Flame spends more time in channel section one, varying with each experiment, lasting between 8 and 12 milliseconds. However, the time that turbulent flame takes to reach the open end is less than 0.7 milliseconds for every experiment. The flame is chaotic in channel section two. Pressure waves, shock waves, local explosions, and DDTs are observed depending on the experiments. Since only a few DDTs occurred during the experiments, all of them will be used to examine the phenomenon and achieve the study's objectives.

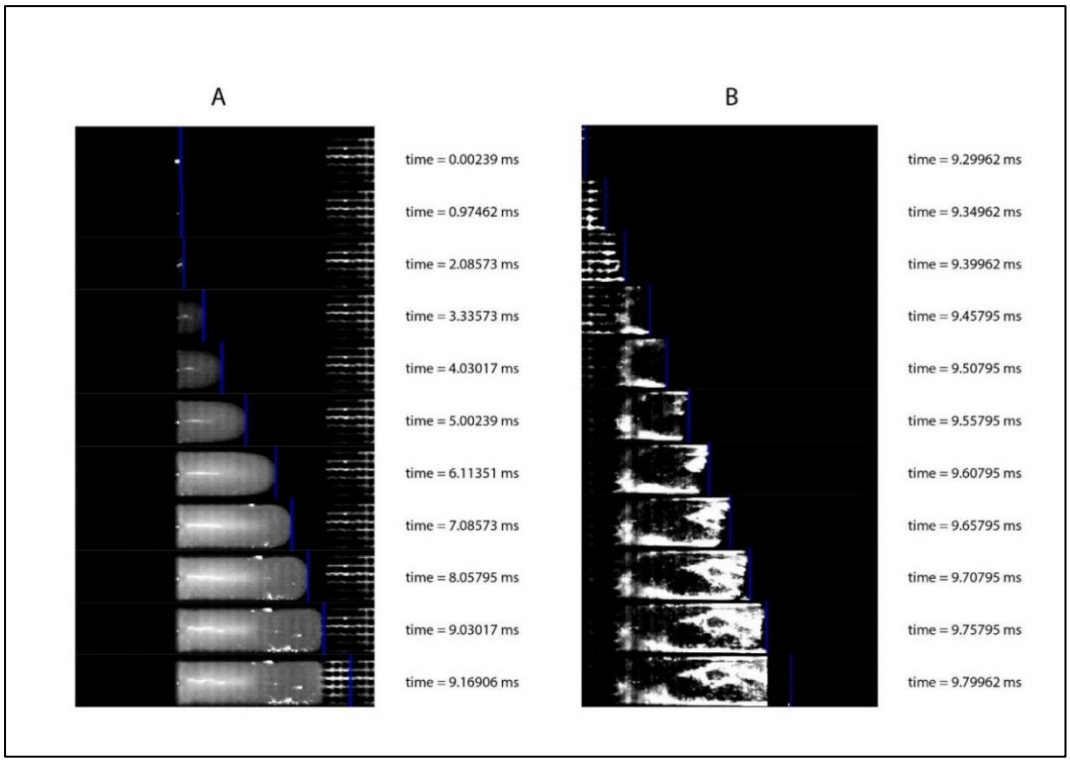

Figure 4.2: Flame position with the time for the experiment in Figure 4.1. A: Flame propagation before obstacles, B: Flame propagation after flame reaching the obstacles.

The pressure sensor two data during the flame propagation at channel section one for equivalence ratio 1.1 is drawn to understand the experimental results and the laminar flame propagation. This is shown in Figure 4.3, and Figures 4.3A and 4.3B show differences between experiments done after and before the repair, respectively. It can be observed that the time taken to build the pressure inside channel section one during flame propagation takes less time after the repair for many experiments. It is also observed that after the repair, flame propagation is consistent in channel section one. However, before the repair, the flame propagation showed inconsistencies in the time it took to reach the obstacles, but the overpressure was similar in many cases for channel section one. Considering this, it is fair to assume the leak affected the results obtained during the experimental study. It could be a reason for the deviations from previously published results on this experimental apparatus. Henriksen et al. [9], [10] observed a 50 to 80 percent probability of detonations in mixtures for the equivalence ratio 1.0 to 1.2. However, this study observed only six detonations out of 40 experiments.

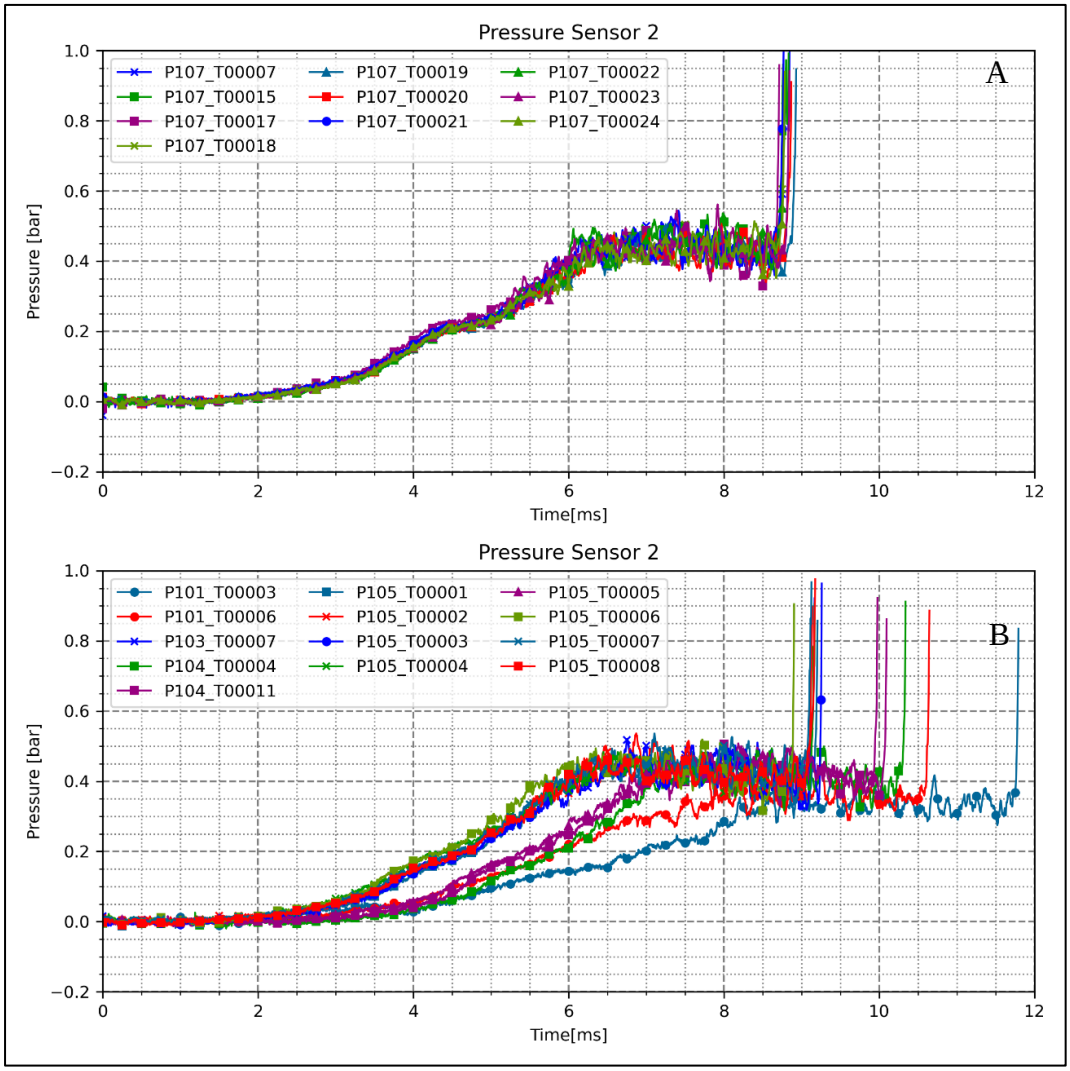

Figure 4.3: Channel section one pressure readings at pressure sensor two for equivalence ratio 1.1 during the flame propagation A) experiments after the repair, B) experiments before the repair

Overpressure at pressure sensor one during laminar flame propagation is shown in Figure 4.4. It shows how the overpressure was changed for the experiments mentioned in Table 4.1. Table 4.4 shows average maximum overpressures during channel section one flame propagation for different equivalence ratios, which show a trend like the mean maximum peak pressures. Maximum values can be observed between equivalence ratios 1.0 to 1.3. The maximum pressures observed at pressure sensor one during laminar flame propagation have similar values for the equivalence ratios 1.0 to 1.3. However, the time it takes to reach the value is different. The overpressure value affects the velocity of the unburnt gas flow and flow regime ahead of the flame through the obstacle array and channel opening. However, observing maximum overpressures, it could be assumed that the leak has not affected the overpressure. The overpressure values before and after the repair show similar values that prove the above assumption.

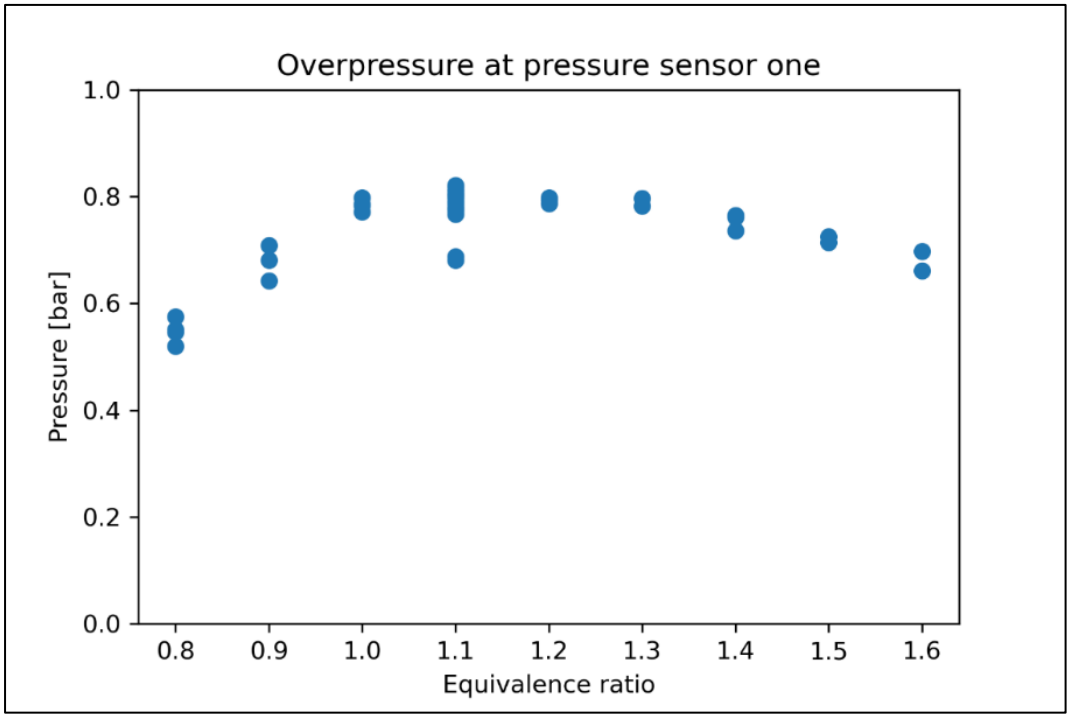

Figure 4.4: Maximum overpressures at pressure sensor one during laminar flame propagation for all experiments in Table 4.1

Knudsen [13] has observed a similar pattern of overpressure during laminar propagation. The hydrogen premixed gas mixtures between 30% and 40% hydrogen volume percentages showed the maximum overpressure for unobstructed 3m pipe. Compared to this study, the trend is similar, and maximum overpressures before obstacles are observed at equivalence ratios of 1.1 to 1.3, where the highest energy release was expected; therefore, the highest overpressures were observed.

Table 4.4: Average maximum pressure at pressure sensor one during laminar flame propagation

Equivalence ratio	**Average maximum overpressure**
0.8	0.55
0.9	0.68
1.0	0.78
1.1	0.79
1.2	0.79
1.3	0.79

1.4	0.76
1.5	0.72
1.6	0.68

4.1.2 Highspeed image data analysis

High-speed image tracking results are used to measure the flame velocities and flame position for channel sections one and two. The velocities obtained from flame tracking will be filtered using the Savitzky-Golay filter in Python (‘*savgol_filter’*). The window length and polynomial order are inputs given to this filter. The window length can affect the mean square error [29]. So, window length was selected as 10% of total data points, and it is considered nine, and polynomial order is considered two for the filtering. Third-degree polynomial fitting is used to understand the velocity trends. The velocity results for the two sections will be analyzed separately for detonation cases to examine the phenomenon.

Figure 4.5 shows the flame speed during laminar flame propagation, flame position, and pressure build-up recorded by pressure sensor one. Figure 4.5A shows pressure recorded by pressure sensor one and flame front position during the same time. 4.5B shows the flame front velocities calculated from raw flame tracking data, filtered velocity curve of the raw values, and third-degree polynomial fitted curve for the experiment P107_T00018.

The filtered flame velocity graph observed that the flame front stayed at zero velocity for two milliseconds and then increased. When the flame nears the obstacles, flame speed drops to a reduced steady value. The initial zero values were due to a flame tracking error reflected on the flame position graph.

During the flame speed increase period, an increase in pressure was observed. This happens because the energy release is high. The expansion of unburnt gas near the flame front pushes the unburnt gas in front of the flame, and forward-flowing gas is trapped due to the obstacles, increasing the pressure in channel section one. This is reflected on the flame position graph in 4.5A, where the maximum pressure value was reached after the flame front passed the pressure sensor one. But when the maximum overpressure was reached, the velocity started to drop. This was explained by Knudsen [13], pressure build-up by the unburnt gas before the flame hinders forward movement, so the flame is flattened and moves radially towards the walls, reducing the burning rates and flame surface. This was why the velocity dropped to a steady value, as shown in the graph when the flame reached the obstacles.

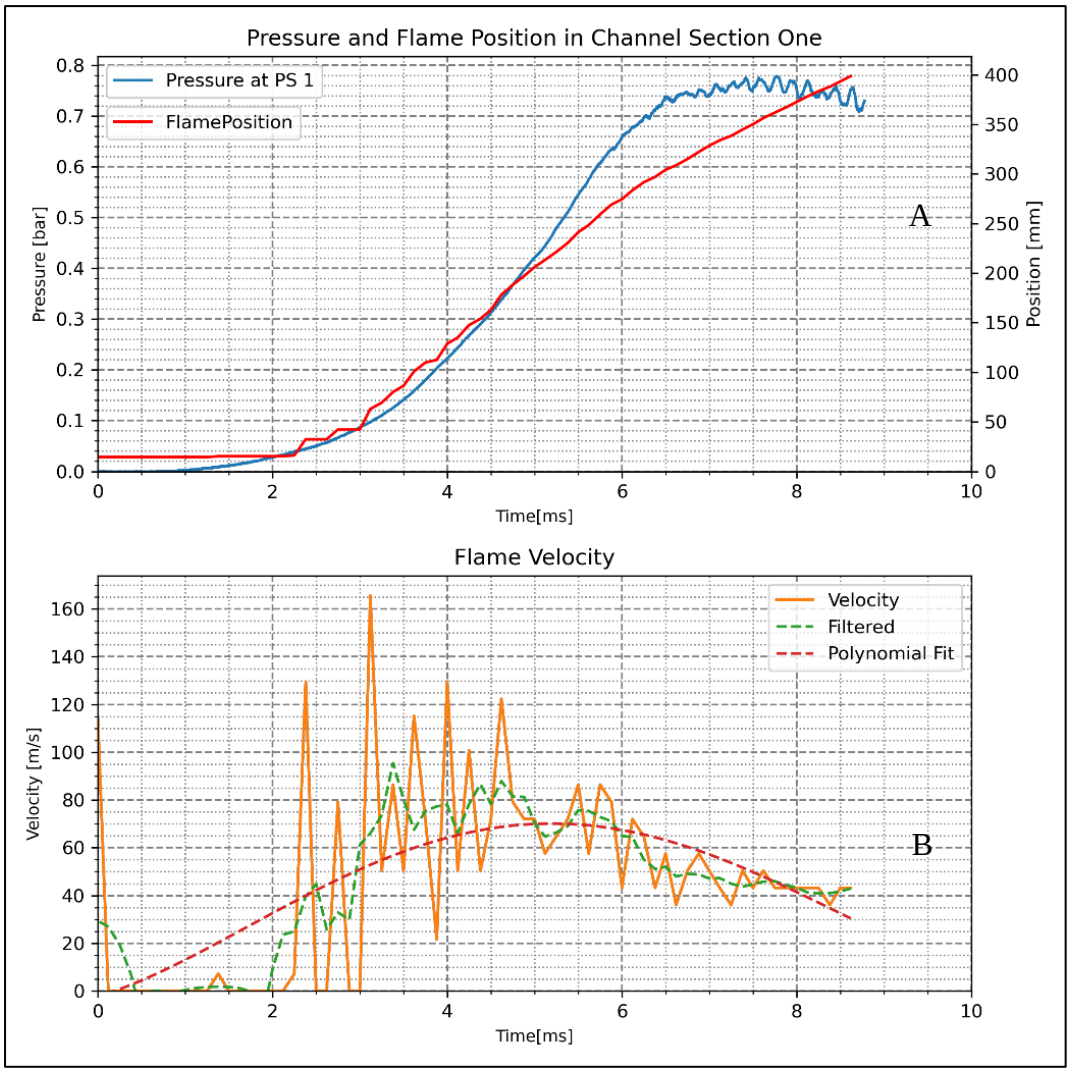

Figure 4.5: P107_T0018 pressure readings at pressure sensor one, flame position, and flame velocity during laminar flame propagation A) graphs of pressure at pressure sensor one and flame position during flame propagation in channel section one, B) graphs of flame front velocities calculated from raw measurements, filtered flame front velocities, and third-degree polynomial fitted velocities

The flame velocity at different flame front positions also shows the above-explained trend where the flame front velocities steady at a reduced value when it reaches the obstacles. It can be observed in Figures 4.6, 4.7, and 4.9. Figures 4.6 and 4.7 show the filtered flame front velocities at different flame front positions for the experiments done for the equivalence ratios 0.9 and 1.0, respectively. Figure 4.9 shows the filtered flame front velocities at different flame front positions for the experiments with detonations. The third-degree polynomial fits of the velocities are also shown in these figures. Graph P101_T00002 in Figure 4.7 shows noise even after the filtering due to flame tracking errors. However, the experiments done for equivalence ratios 0.9, 1.0, and 1.1 show that flame front velocities at channel section one are slightly higher in slightly richer mixtures. However, this is not a significant difference.

Experiments done before the repair show inconsistency in velocity trends. Figure 4.6 shows that flame front velocities along channel section one have lower values in experiments done before the repair for equivalence ratio 0.9. However, the opposite trend is shown for the

equivalence ratio of 1.0. Figure 4.8 shows the time the flame front takes to reach the obstacle array during the flame propagation in channel section one. It can be observed that there was a random nature of the flame propagation before the repair and consistent flame propagation after the repair. The inconsistencies of flame front velocities before the repair may have affected the outcome of the experiments. However, there was not enough evidence to conclude that this random nature affected the low number of DDTs since only four experiments out of 28 were detonated after the repair, and only two were detonated before the repair out of 84 experiments. It is difficult to build a definite reason for the lack of DDTs.

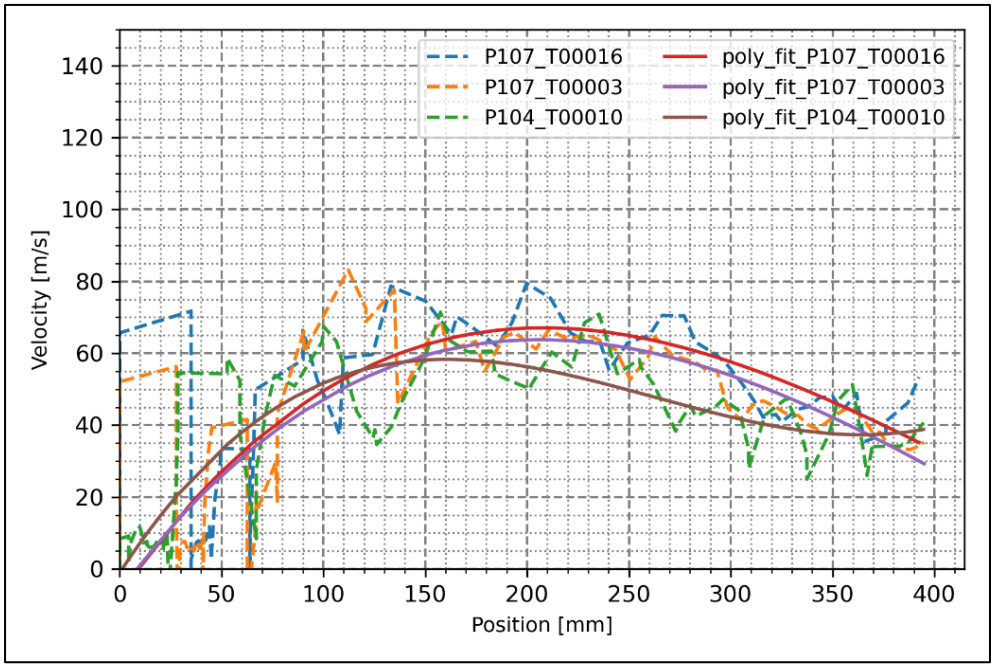

Figure 4.6: Flame front velocity in channel section one for the experiments done for the equivalence ratio of 0.9

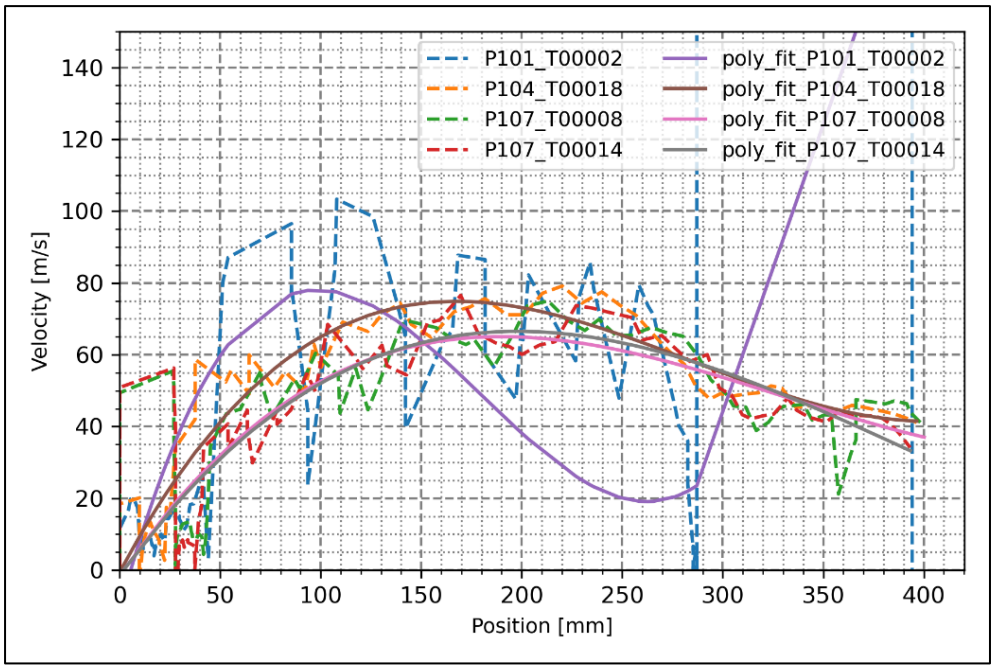

Figure 4.7: Flame front velocity in channel section one for the experiments done for the equivalence ratio of 1.0

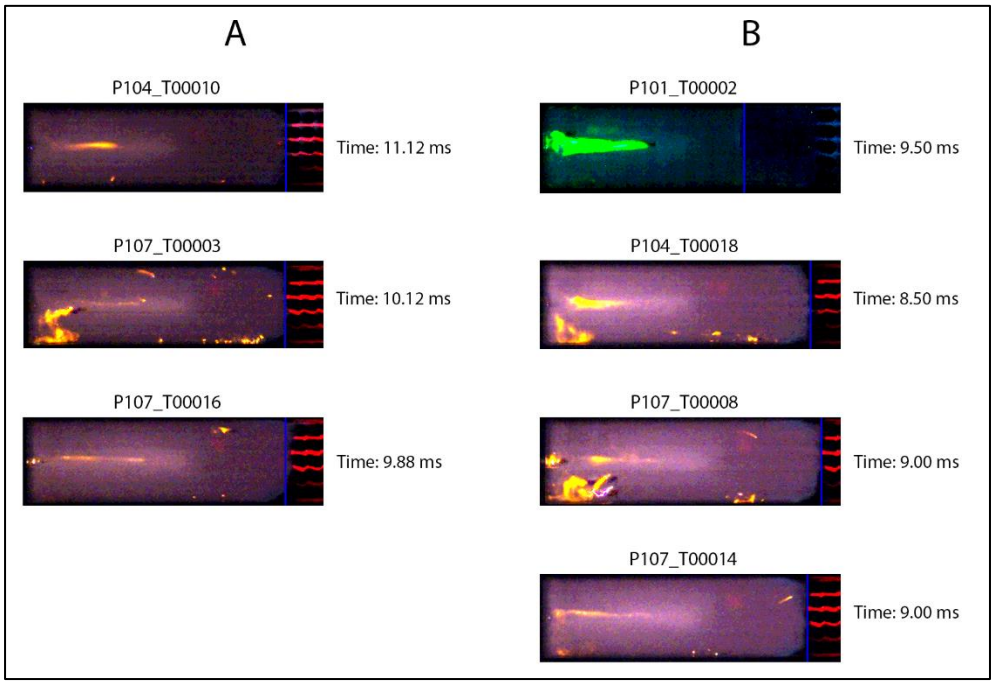

Figure 4.8: Time taken by flame fronts to reach the obstacles in experiments with equivalence ratios 0.9 and 1.0

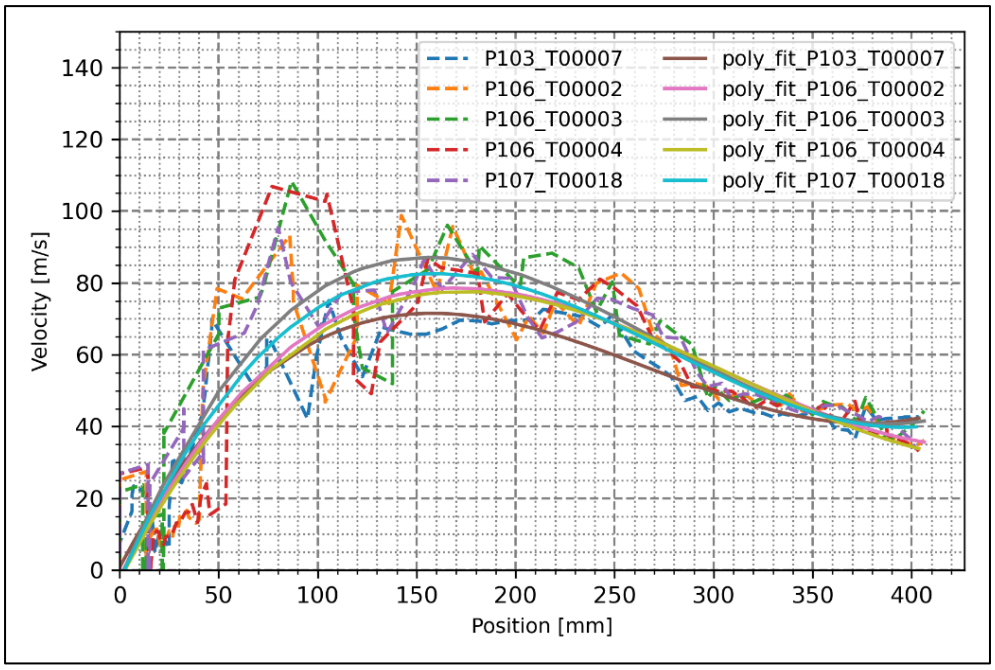

Figure 4.9: Flame front velocities during the laminar flame propagation for experiments with DDT

Figure 4.10 shows the flame front velocity, flame front position, and the pressures at pressure sensors two, three, and four in channel section two during the flame propagation for the experiment P107_T00018. Figure 4.10 B was drawn considering that the flame starts at the end of the obstacle array. Velocity calculated from flame tracking, filtered velocities, and third-degree polynomial fit of the calculated velocities is shown in the flame velocity plot. Raw pressure data for pressure sensors two, three, and four is shown in the pressure at pressure sensors 2, 3, & 4 plot. It is shown in Figure 4.10 B that the velocity is considerably low initially and increases until the flame front reaches the open end. However, the initial reduced values are due to errors in the flame-tracking algorithm. It is shown in the flame position graph in the initial 0.09 milliseconds. When flame leaves the obstacle array, it already has a velocity, and the flame regime is turbulent, so the flame velocity can be considered a higher value. A constant increase in flame front velocity was not observed in every experiment. This behavior was observed in detonated cases, as shown in Figure 4.13.

However, considering the trends from third-degree polynomial fits, the flame front velocity increases initially and then decreases slightly or keeps steady until the flame front reaches the open end. This trend shows that the flame front speed increases until the flame reaches 750mm to 850mm. This pattern is shown in many experiments and can be observed in Figures 4.11, 4.12, and 4.13. Figures 4.11 and 4.12 show the filtered flame front velocities calculated from flame tracking and fitted curve for velocities using third-degree polynomial curve fitting for the flame propagation at channel section two for experiments with equivalence ratios 0.9 and 1.0, respectively. Figure 4.13 shows the same graphs for DDT observed cases. Both plots do not show any significant differences in flame front velocities for the experiments before and after the repair. Considering this, it is safe to assume that the leak has not affected the flame propagation in channel section two.

Increasing flame front velocity is observed in both plots until the flame reaches 750mm to 850mm. This suggests that a higher reaction rate and higher energy release in the flame is expected when the flame speed increases, which could increase the pressure in front of the flame. The peak pressures observed by pressure sensor four are higher compared to pressure sensor three. The increasing flame speed could explain the trend shown by the peak pressures. Increasing flame front velocities were observed even after passing the pressure sensor three positions, which is 650mm from the ignition source. This was the most likely reason for the higher pressures recorded by the pressure sensor four.

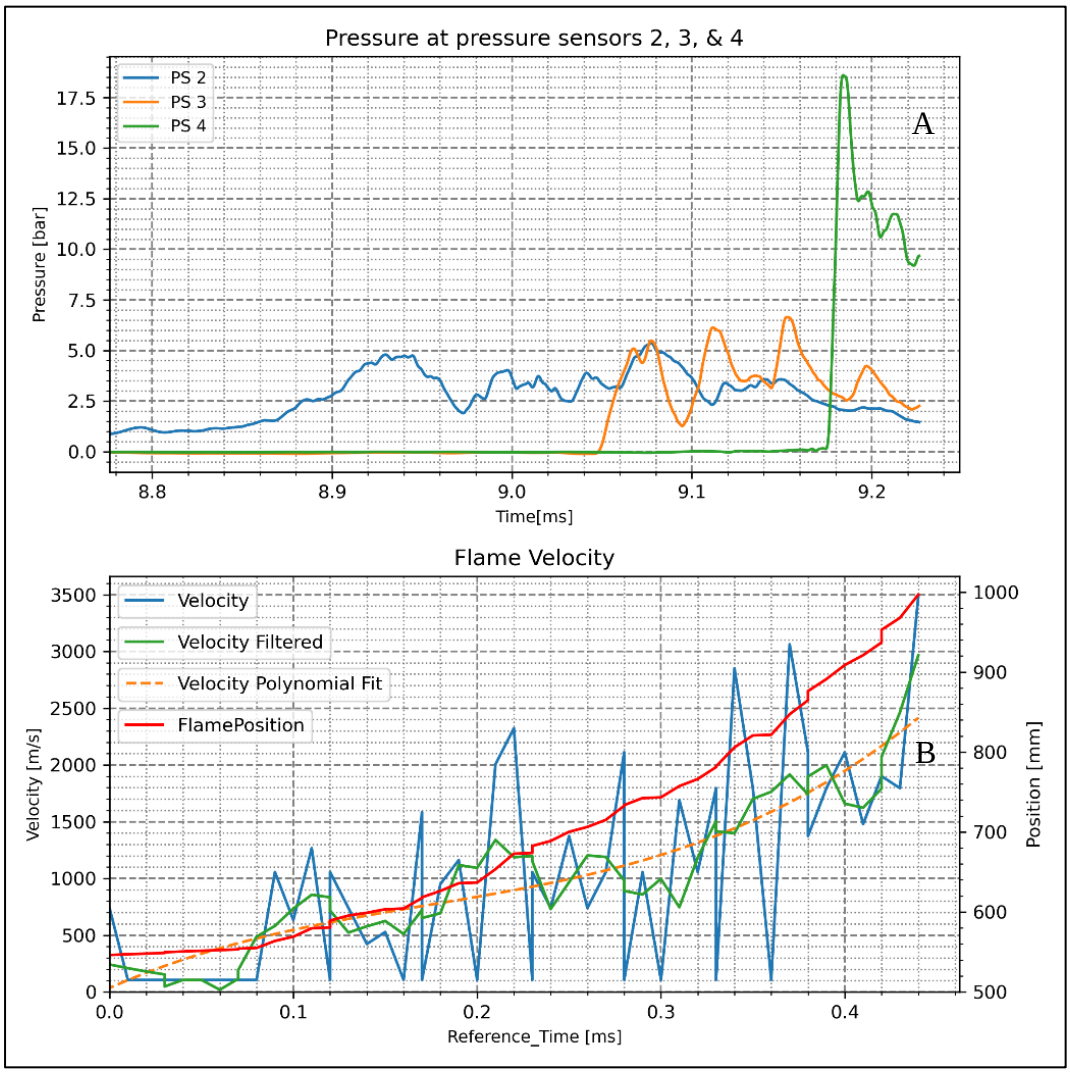

Figure 4.10: P107_T0018 pressure readings, flame front velocity, and flame front position during flame propagation in channel section two, A) pressure readings at pressure sensors 2, 3, and 4, B) Flame front position and flame front velocity

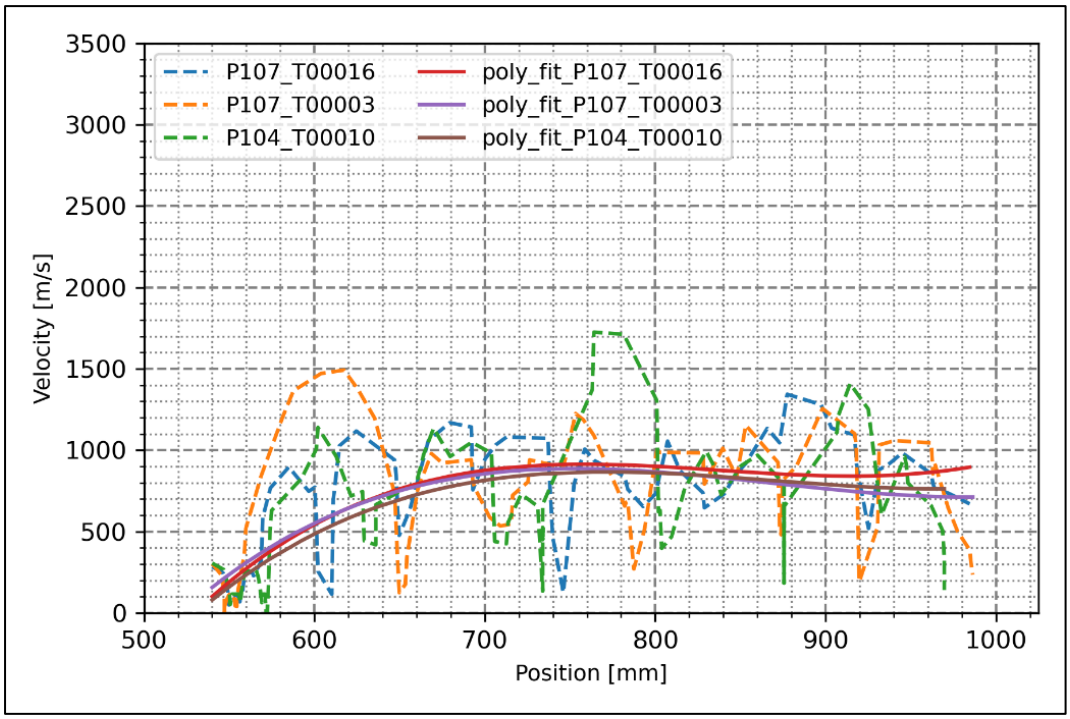

Figure 4.11: Flame front velocity along the channel in channel section two for the experiments done for the equivalence ratio of 0.9

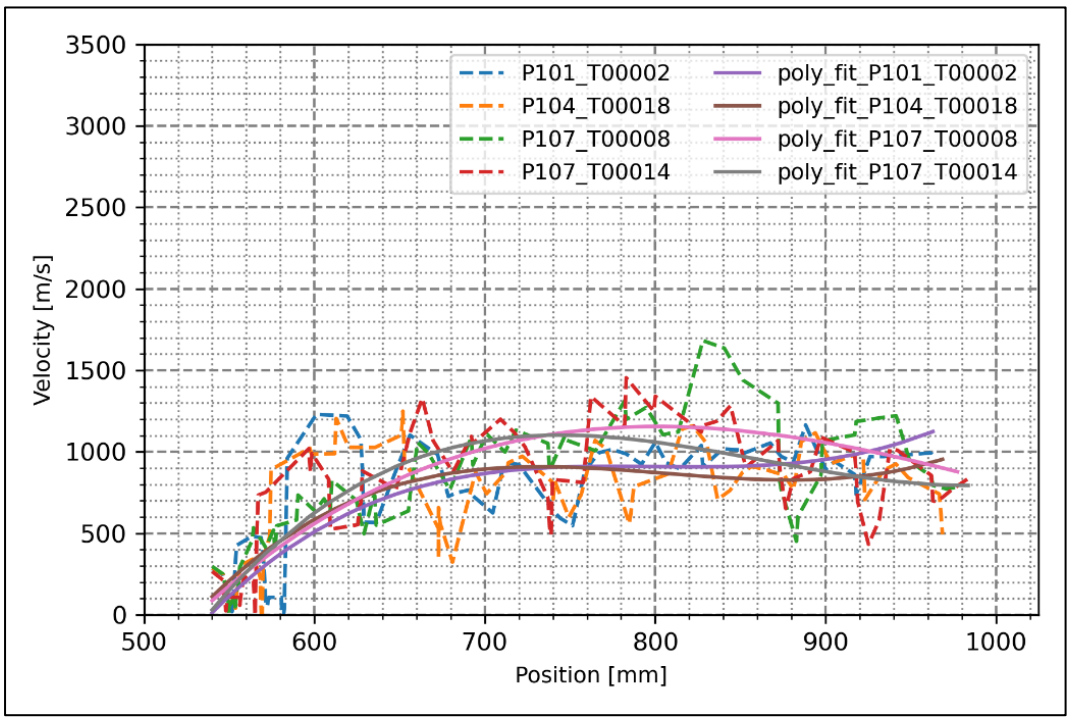

Figure 4.12: Flame front along the channel in channel section two for experiments done for equivalence ratio 1.0

Figure 4.13 shows the flame front speed in channel section two for the experiments that observed DDT. It is observed that the velocities here reach 1900 ms^{-1} and, in some cases, reach 2000 ms^{-1}, which shows that during the detonations, flame front velocities reach CJ velocity for the hydrogen-air premixed combustion. The CJ velocity for hydrogen-air mixtures with initial conditions at 25 ^{o}C and 1 atm pressure is 1968 $ms^{-1,}$ and the values observed here are near this value. It could be considered that the flame reached the CJ detonation velocity, suggesting that the detonations had occurred.

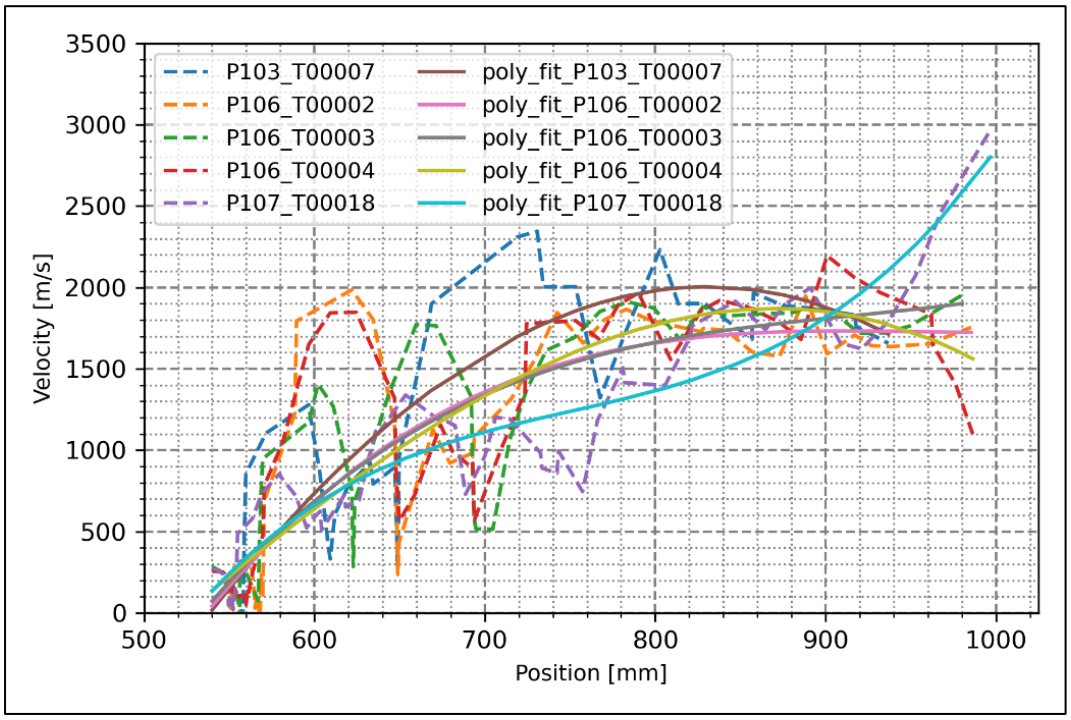

Figure 4.13: Flame front velocities along the channel in channel section two for experiments with DDT

4.1.2.1 Kirana images

Schlieren images obtained from the experiments can be used to explain observations during the flame propagation. Flame propagation with different regimes is a vital part of DDT. A laminar flame transitioning to a wrinkled flame due to instabilities is one of the stages of flame propagation, and it is observed here before the flame enters the obstacle array. This was observed in the images taken from Kirana. Figure 4.14 shows the Schlieren. However, distinguishing the instabilities that occurred here was difficult since it appears to be an aggregate of several instabilities. However, there might be diffusive thermal instability and hydrodynamic instability of Rayleigh-Taylor instability present here. The burnt gas or the flame is lighter than the unburnt gas, so lighter fluid could accelerate towards unburnt gas, which would create hydrodynamic instability.

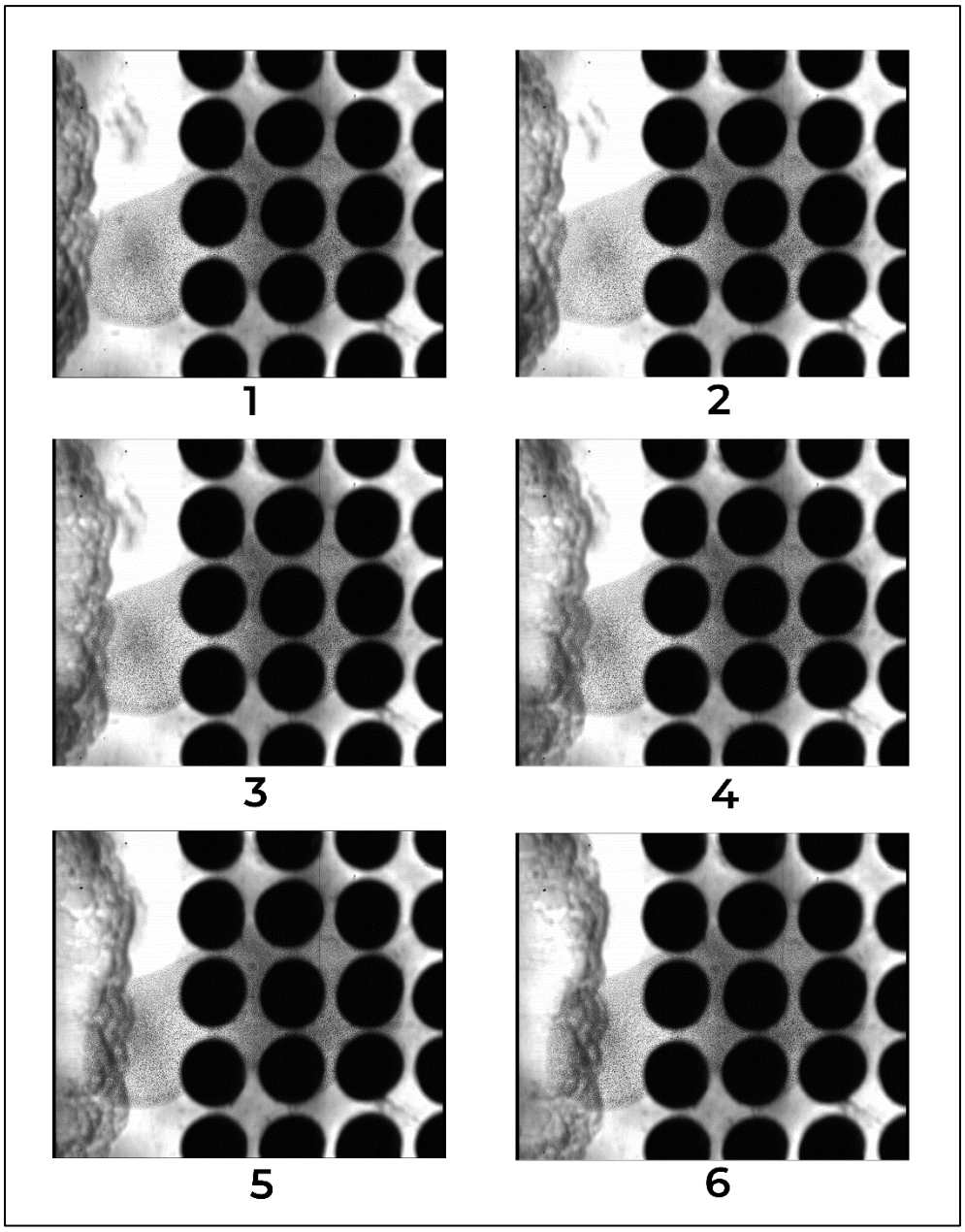

Figure 4.14: Kirana images for the flame propagation before the obstacles

4.1.2.2 Detonations and hotspot

Analyzing image data from detonated cases shows the hotspot observed by Henriksen et al. [9], [10] during DDTs. The propagation of DDT at channel section two starts with the formation of the hotspot. The hotspot is always formed in the middle of the channel and propagates in different directions before transitioning into a local explosion. Then, it was transitioned to a detonation flame front. The direction in which the hotspot travels can be either the top wall, the bottom wall, or the middle of the channel. The images show a two-dimensional view; thus, the hotspot could move towards a side wall and initiate the local explosion. However, this cannot be confirmed without image data on depth. Figures 4.15 and 4.16 show hotspot formation and transition to detonation for the experiments that observed detonations.

Figures 4.15 a, 4.15 c, and 4.16 e show the instances where formed hotspots move in the middle and convert to detonations. Figure 4.15 b shows a detonation occurring at the top wall, while Figure 4.16 d shows the transition occurring at the bottom wall. Figures a), c), and e) show the hotspot formation at 692.10 mm, 692.10 mm, and 732.72 mm from the ignition source, respectively. Figures b) and d) show the hotspot formation at 694.80 mm and 730.80 mm from the ignition source, respectively. The hotspot formation is also random since the distance where the hotspot is observed is different for every detonated case. The formation of a hotspot could be due to the coupling of the shock and flame. However, this is difficult to determine and examine due to the lesser number of detonation occurrences and random behavior of the occurred DDTs. Henriksen et al [9], [10] suggest that the hotspot formation could be due to the collision of two pressure waves exiting from the top and bottom of the channel. However, this could not be examined thoroughly due to a lack of detonations during experiments.

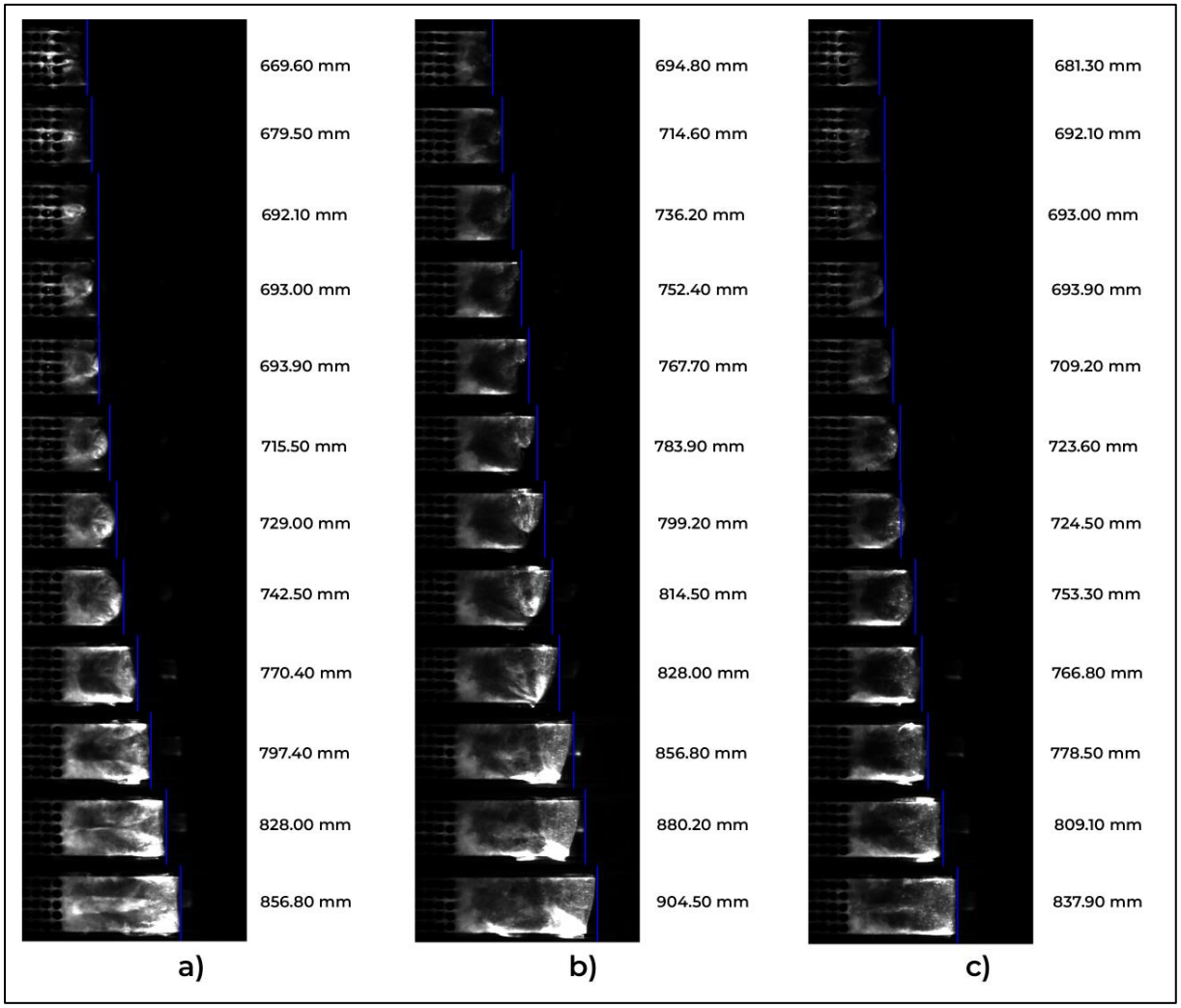

Figure 4.15: Flame propagation in channel section two for the experiments where detonations were observed during P106. a) P106_T00002, b) P106_T00003, c) P106_T00004

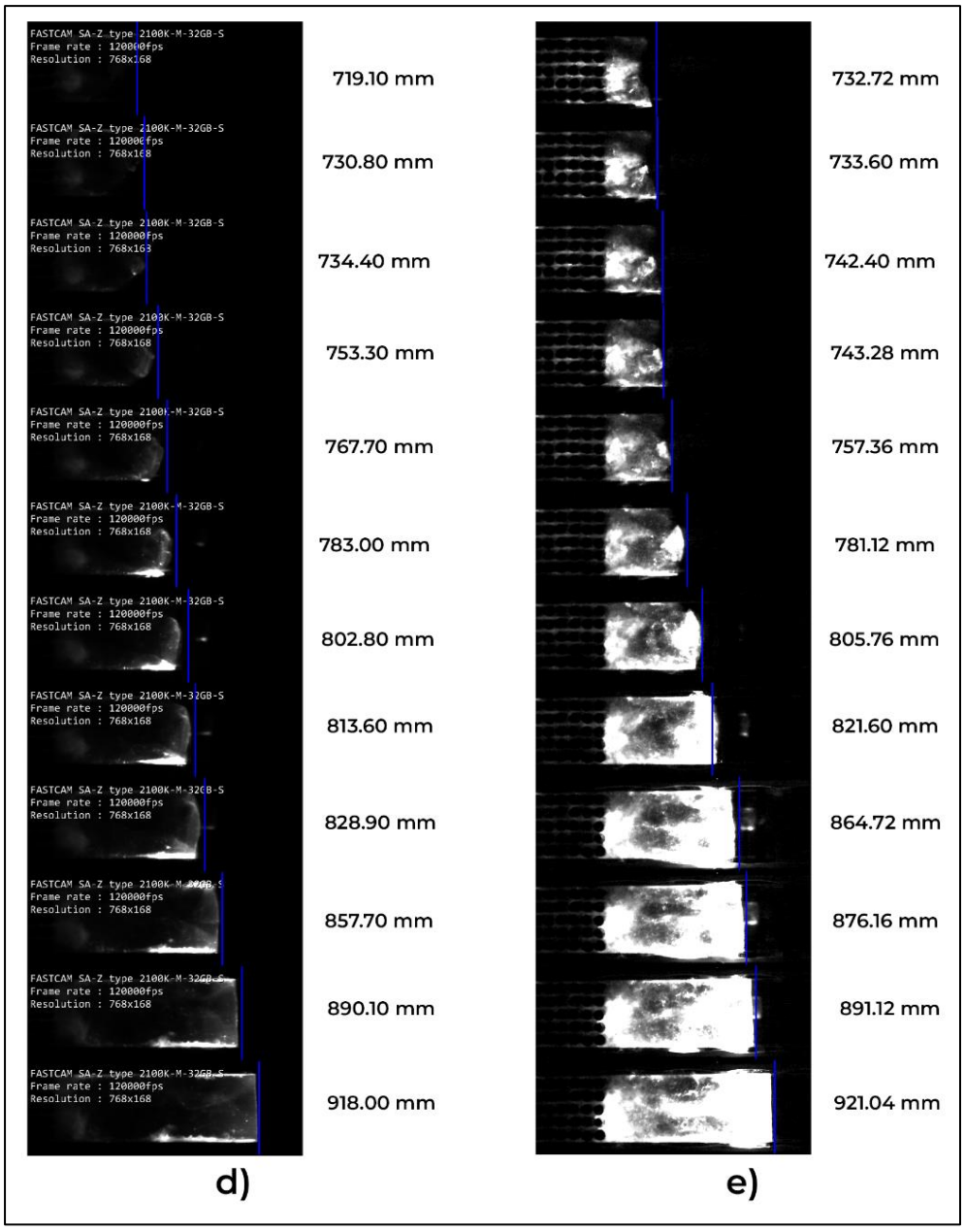

Figure 4.16: Flame propagation in channel section two for the experiments where detonations were observed during P103 and P107. d) P103_T00007, d) P107_T00018

4.2 Comparison and validation

This subchapter compares the results obtained and discusses similarities and deviations between this study and previous studies.

Henriksen et al. [10] observed many DDTs during the same experiment. Experiments were conducted for equivalence ratios 0.9 to 1.5, and 34 detonations were observed from 78 experiments. The equivalence ratios 1.0, 1.1, and 1.2 were detonated with 78%, 80%, and 50% probabilities, respectively. However, during this study, detonations were observed only for equivalence ratio 1.1, and they occurred with a 15% probability. This is a significantly low

value; the only differences observed in these experiments are the leak and the new trigger unit. However, it was impossible to run experiments with the previously used trigger unit during the experiments since it was attached to another experiment. Whether or not it influenced detonations must be evaluated in future studies to confirm this observation. However, the previous study by Henriksen et al. showed the highest probability at a 1.1 equivalence ratio, and this study also showed detonations for the same equivalence ratio.

Gaathaug [8] has presented that the run-up distance where DDT occurs depends on the concentration. The run-up distance was measured from the obstacles to the occurrence point of DDT. The study showed that the run-up distance decreased with increasing hydrogen concentration, possibly due to the high reactivity of slightly richer hydrogen concentrations. However, the run-up distances observed by Gaathaug were more than 300 mm from the obstacles. This study observed DDTs within very short distances from the obstacles. More DDTs could have been observed if the channel had been longer after the obstacles. Gaathaug's study observed DDT at the top of the channel wall. However, this study observed DDT mainly in the middle of the channel, but DDT happened once each at the top and bottom walls. This suggests that the phenomenon is highly random. Gaathaug's study observed detonations for the blockage ratio 0.75 at slightly richer mixtures. This shows the same trend as this study, in which detonations were only observed in slightly richer mixtures.

Maximum peak pressures observed for Henriksen et al. [9] shows similar values obtained in this experiment. However, the peak pressures observed by pressure sensor three were higher than the peak pressures observed by sensor four in Henriksen's study [9]. In this study, peak pressures observed by pressure sensor four are higher than those observed by pressure sensor three, and the increasing velocities during flame propagation can explain this. Gaathaug's [8] study shows similar maximum peak pressures for the detonated cases in 0.75 blockage ratios to this study, and similar observations can be made for the experiments done in Knudsen's study [13] for blockage 0.782, where detonations are observed. Both studies recorded pressures above 1.5 MPa for the detonated cases, similar to observations made in this study, and they are above CJ detonation pressure.

Henriksen et al. [9], [10] observed hotspot in the detonated cases and similar observations were made during this study. However, the observed hotspot behaves very randomly, and understanding a pattern or reason for the occurrence was difficult during the study. The study of Henriksen et al.[9], [10] hypothesizes that this hotspot may occur due to the collision of shockwaves. However, the exact reason for the phenomenon was not found. This study was also unable to examine the hotspot formation due to a lack of detonations.

4.3 Error sources

This subchapter briefly discusses causes assumed to be the main error sources in this experimental study. The gas handling unit, data post-processing, and leaks observed in the explosion channel were identified as potential error sources, and they were further discussed here to understand their effect on results.

Gas handling unit

Premixed hydrogen and air are supplied to the explosion channel through two Coriolis flow meters before premixing. The mass flow rates were calculated and fixed according to the desired equivalence ratios, and the desired flow rates will be achieved by manually controlling the valves. The filling was done for 300 seconds, and the actual equivalence ratio was calculated by considering the latter part of the flow meter readings received and recorded by the oscilloscope. However, manual controlling is done using the display of the Coriolis meter, which has a lag in response. This can be observed in Figures 4.17 and 4.18 as sudden concentration changes. The steadiness of the mass flow is important, and averaging the recorded flow rate could affect the calculated actual equivalence ratio. This could be an error during the experiment and an error source of post-processing. Thus, during the analysis of the results, the experiments with an error of more than ± 0.035 from the intended equivalence ratio were neglected.

Leak and repair

Hydrogen concentration inside the channel due to leaks was another uncertainty during the experiments. However, after the channel was repaired, the hydrogen concentration was checked using hydrogen sensors. The concentration check revealed that the concentration inside the channel remained steady after the repair. However, before the repair, it was uncertain whether the concentration of the inside channel remained steady and whether the leak could have affected the results during the flame propagation. Figures 4.17 and 4.18 show the results obtained during the concentration test. The values go to zero at the start and end of the concentration test. It shows that the concentration is steady, and it takes several seconds to reduce the concentration after the lid drops, and figures show that this does not affect the concentration inside the channel. However, even with correct concentration inside the channel, DDTs were not observed in experiments done under P107. Considering this, it is hard to conclude that the leak was the only source that caused the low number of detonations.

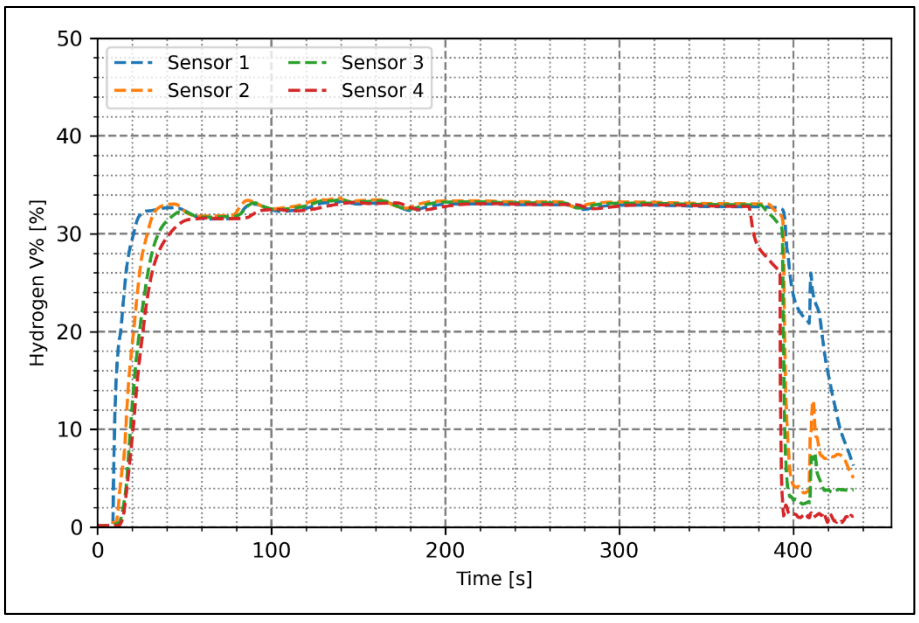

Figure 4.17: Hydrogen concentration test results for equivalence ratio 1.1

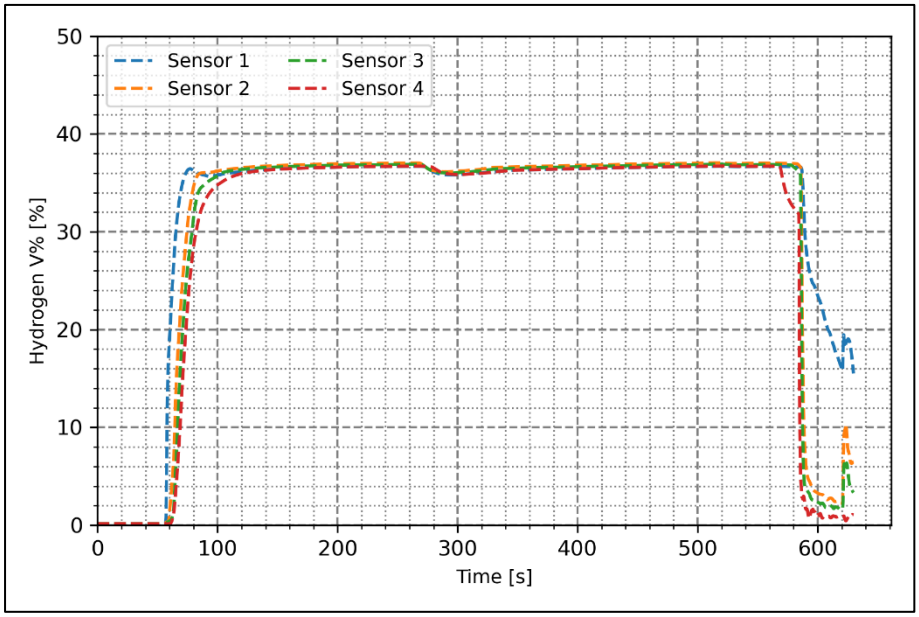

Figure 4.18: Hydrogen concentration test results for equivalence ratio 1.3

Post-processing

Another potential error source could be post-processing. Some uncertainties were observed during image processing and flame tracking, which could affect the calculated velocity values. However, most of the results obtained from the flame front tracking showed correct results. Pressure post-processing showed uncertainties by identifying incorrect trigger signal in some experiments. However, this was corrected during the analysis of the results by comparing it with image data.

Other sources

Another uncertainty about the gas mixture was that the temperature was assumed to be 25 ^{o}C. However, running the experiments several times could increase the channel wall temperature due to the energy released during explosions. Thus, the gas's initial temperature could be slightly higher inside the channel. Flushing the system after every experiment using air could reduce this effect by reducing the channel temperature. However, this may have caused errors to a certain level.

5 Conclusion

Flame propagation and transition to different combustion regimes are important for DDT in premixed combustion and gas explosions. This study shows how flame propagation is an important aspect of DDT. Ignition, laminar flame propagation, laminar flame propagation with instabilities, turbulent flame propagation, and detonations were observed during the one-meter channel experiments. Detonations are most probable to occur with slightly richer mixtures. The experimental study only observed detonations for an equivalence ratio of 1.1.

The maximum peak pressures for detonated cases show pressures above CJ detonation pressure. Maximum peak pressures for deflagration cases show that the highest peak pressures observed are around equivalence ratios of 1.0 to 1.3, which shows that the highest energy release happens in slightly richer mixtures. The velocities observed in detonated experiments were between 1800 ms^{-1} and 2000 $ms^{-1,}$ which is close to the CJ detonation velocity that confirms the detonations. Deflagration cases show flame propagation velocities lower than CJ velocities.

The formation of a hotspot in detonations was observed in every case. However, the deflagrations don't show a hotspot, which suggests that a hotspot is a unique attribute of DDT. The propagation of the hotspot was random; it could transition into a detonation at the top wall, bottom wall, or middle of the channel. The distance from the obstacles to the hotspot formation is also random; however, in most cases, this happened within 200mm from the obstacle array.

During the experimental study, a leak was observed. This affected the flame propagation inside the channel by affecting the flame propagation velocities. The leak didn't affect the overpressure buildup inside the channel. The detonated cases in this experimental study were significantly lower than in the previous studies done in this setup. The results gathered before and after the repair of the explosion channel show differences. However, concluding that the leak affected the DDT is insufficient.

Experiments were conducted with several equivalence ratios, and the highest peak pressures were observed only around equivalence ratios 1.0 to 1.3. This suggests that the highest energy release was around these equivalence ratios, with the highest probability of DDT. Future experimental studies could focus on these equivalence ratios to analyze the DDT further.

6 Suggestions for future study

Based on the findings of this thesis study, several future research studies could be suggested.

As discussed previously, considering the changes made to the experimental setup by introducing the new trigger system could have affected DDT. As a future study on this experimental setup, it would be better to check whether this trigger unit affects the occurrence of DDT.

The leak could have caused the lack of DDTs by creating randomness in the flame propagation. A future study will be beneficial to check this to see how inconsistencies and consistencies affected the occurrence of DDTs.

One of the objectives of this experimental study was to examine DDT and find reasons for the hotspot formation. However, the lack of detonations prevented this objective from being fulfilled and changed the study's objectives. Future studies could be used in this experimental setup to examine the hotspot formation further.

References

[1] W. L. Jolly, “Hydrogen | Properties, Uses, & Facts | Britannica.” Accessed: Mar. 06, 2024. [Online]. Available: https://www.britannica.com/science/hydrogen

[2] “IEA – International Energy Agency,” IEA. Accessed: Mar. 06, 2024. [Online]. Available: https://www.iea.org

[3] D. S. Burgess and M. G. Zabetakis, *Detonation of a Flammable Cloud Following a Propane Pipeline Break: The December 9, 1970, Explosion in Port Hudson, Mo*. U.S. Department of Interior, Bureau of Mines, 1973.

[4] A. Mjaavatten and D. Bjerketvedt, “A Hydrogen-Air Explosion in a Process Plant: A Case History,” Sep. 2005, Accessed: Mar. 07, 2024. [Online]. Available: https://www.h2knowledgecentre.com/content/conference176

[5] D. Bradley, G. A. Chamberlain, and D. D. Drysdale, “Large vapour cloud explosions, with particular reference to that at Buncefield,” *Philosophical Transactions of the Royal Society A: Mathematical, Physical and Engineering Sciences*, vol. 370, no. 1960, pp. 544–566, Feb. 2012, doi: 10.1098/rsta.2011.0419.

[6] M. Kolberg, “Eksplosjon ved hydrogenstasjon,” NRK. Accessed: Mar. 13, 2024. [Online]. Available: https://www.nrk.no/norge/eksplosjon-ved-hydrogenstasjon-1.14582914

[7] W. I. Inc, “Case Study: Power Plant Hydrogen Explosion,” WHA International, Inc. Accessed: Mar. 13, 2024. [Online]. Available: https://wha-international.com/case-study-power-plant-hydrogen-explosion/

[8] A. V. Gaathaug, “Experimental Study of Deflagration to Detonation Transition in Hydrogen-Air Mixtures,” Doctoral thesis, Telemark University College, 2015. Accessed: Jan. 21, 2024. [Online]. Available: https://openarchive.usn.no/usn-xmlui/handle/11250/2437782

[9] M. Henriksen, K. Vaagsaether, and D. Bjerketvedt, “Deflagration-to Detonation Transition of Hydrogen-Air Mixture in a Highly Congested, Open-ended Channel,”

[10] M. Henriksen, A. Pykhtina, V. A. Gaathaug, K. Vaagsaether, and D. Bjerketvedt, “A Study of The Deflagration-To-Detonation Transition and Its Limits of Hydrogen-Air Mixtures in An Open-Ended, Obstructed Channel,” presented at the ICDERS, Jul. 2023.

[11] M. Henriksen, “A study of premixed combustion of gas vented from failed Li-ion batteries,” Doctoral thesis, University of South-Eastern Norway, 2021. Accessed: Jan. 21, 2024. [Online]. Available: https://openarchive.usn.no/usn-xmlui/handle/11250/2829351

[12] M. Henriksen, K. Vaagsaether, J. Lundberg, S. Forseth, and D. Bjerketvedt, “Numerical study of premixed gas explosion in a 1-m channel partly filled with 18650 cell-like cylinders with experiments,” *Journal of Loss Prevention in the Process Industries*, vol. 77, p. 104761, Jul. 2022, doi: 10.1016/j.jlp.2022.104761.

[13] V. Knudsen, “Hydrogen gas explosions in pipelines, modeling and experimental investigations,” Doctoral thesis, Telemark University College, 2006. Accessed: Mar. 18, 2024. [Online]. Available: https://openarchive.usn.no/usn-xmlui/handle/11250/2438582

[14] S. McAllister, J.-Y. Chen, and A. C. Fernandez-Pello, *Fundamentals of Combustion Processes*. New York, GERMANY: Springer, 2011. Accessed: Mar. 18, 2024. [Online]. Available: http://ebookcentral.proquest.com/lib/ucsn-ebooks/detail.action?docID=972076

[15] I. Glassman, *Combustion*. San Diego, UNITED STATES: Elsevier Science & Technology, 1996. Accessed: Mar. 27, 2024. [Online]. Available: http://ebookcentral.proquest.com/lib/ucsn-ebooks/detail.action?docID=331918

[16] A. V. Gaathaug, "Flame propagation in a transparent pipe with a single obstruction."

[17] M. Barrère and F. A. Williams, "Comparison of combustion instabilities found in various types of combustion chambers," *Symposium (International) on Combustion*, vol. 12, no. 1, pp. 169–181, Jan. 1969, doi: 10.1016/S0082-0784(69)80401-7.

[18] C. K. Law, *Combustion physics*. Cambridge ; New York: Cambridge University Press, 2006.

[19] L. Boeck, "Deflagration-to-Detonation Transition and Detonation Propagation in H2-Air Mixtures with Transverse Concentration Gradients," 2015.

[20] N. Dimela, "Numerical simulations of primary break-up in two-phase flows," 2017. doi: 10.13140/RG.2.2.27248.71681.

[21] K. K. Kuo, *Principles of combustion*. in A Wiley-Interscience publication. New York: Wiley, 1986.

[22] S. B. Dorofeev, M. S. Kuznetsov, V. I. Alekseev, A. A. Efimenko, and W. Breitung, "Evaluation of limits for effective flame acceleration in hydrogen mixtures," *Journal of Loss Prevention in the Process Industries*, vol. 14, no. 6, pp. 583–589, Nov. 2001, doi: 10.1016/S0950-4230(01)00050-X.

[23] D. Bjerketvedt, J. R. Bakke, and K. van Wingerden, "Gas explosion handbook," *Journal of Hazardous Materials*, vol. 52, no. 1, pp. 1–150, Jan. 1997, doi: 10.1016/S0304-3894(97)81620-2.

[24] R. Porowski and A. Teodorczyk, "Cellular Structure of Detonation Wave for Hydrogen-Methane-Air Mixtures," Jan. 2011.

[25] E. S. Oran and V. N. Gamezo, "Origins of the deflagration-to-detonation transition in gas-phase combustion," *Combustion and Flame*, vol. 148, no. 1, pp. 4–47, Jan. 2007, doi: 10.1016/j.combustflame.2006.07.010.

[26] G. D. Roy, S. M. Frolov, A. A. Borisov, and D. W. Netzer, "Pulse detonation propulsion: challenges, current status, and future perspective," *Progress in Energy and Combustion Science*, vol. 30, no. 6, pp. 545–672, Jan. 2004, doi: 10.1016/j.pecs.2004.05.001.

[27] P. A. Urtiew, A. K. Oppenheim, and S. O. Saunders, "Experimental observations of the transition to detonation in an explosive gas," *Proceedings of the Royal Society of London. Series A. Mathematical and Physical Sciences*, vol. 295, no. 1440, pp. 13–28, Jan. 1997, doi: 10.1098/rspa.1966.0223.

[28] Abraham. Savitzky and M. J. E. Golay, "Smoothing and Differentiation of Data by Simplified Least Squares Procedures.," *Anal. Chem.*, vol. 36, no. 8, pp. 1627–1639, Jul. 1964, doi: 10.1021/ac60214a047.

[29] M. Sadeghi and F. Behnia, “Optimum window length of Savitzky-Golay filters with arbitrary order”.

Appendices

Appendix A: Task description

Appendix B: Extended experimental matrix

Appendix C: Maximum peak pressures observed in experiments used for the result analysis

Appendix D: Maximum overpressures observed in channel section one

Appendix A: Task description

Faculty of Technology, Natural Sciences and Maritime Sciences, Campus Porsgrunn

FMH606 Master Thesis

Title: Experimental Study of DDT of Hydrogen-Air Gas Explosion

USN supervisor: Assoc Prof. Mathias Henriksen (USN), Prof. Dag Bjerketvedt (USN), Ph.D. Petar Bosnic (USN)

External partner: Hydrogeni (FME Research Center)

Task background:

Hydrogen has become increasingly popular as an alternative fuel and storing renewable energy. However, hydrogen poses an explosion hazard since it has a low minimum ignition energy and is highly laminar burning velocity; thus, it can potentially cause severe damage to infrastructure and humans. The main task of this project is to study the deflagration to detonation transition (DDT) of hydrogen-air mixtures in a 1-meter obstructed channel.

Task description:

- Formulate Problem Descriptions
- Literature review on DDT of hydrogen-air explosions
- Conduct experiments of hydrogen-air explosion in the laboratory
- Compare experimental results to CFD results (optional)

Student category: EET and PT students

Is the task suitable for online students (not present at the campus)? No

Practical arrangements:

Experiments in USN-laboratory Porsgrunn

Supervision:

As a general rule, the student is entitled to 15-20 hours of supervision. This includes the necessary time for the supervisor to prepare for supervision meetings (reading material to be discussed, etc).

Signatures:

Supervisor (date and signature):

Students (write clearly in all capitalized letters): ATTANAYAKE MUDIYANSELAGE CHINTHAKA ATTANAYAKE

Students (date and signature):

Appendix B: Experimental matrix – extended version

Experiment Name	Ignition (Y/N)	Post Processing (Y/N)	DDT (Y/N)	Measured Equivalence Ratio	Intended Equivalence Ratio	Experiment Name (within ±0.035 error of phi)
P101_T00001	Y	N	N		0.9	P101_T00002
P101_T00002	Y	Y	N	0.984	1.0	P101_T00003
P101_T00003	Y	Y	N	1.103	1.1	P101_T00006
P101_T00004	Y	Y	N	1.163	1.2	P102_T00002
P101_T00005	Y	Y	N	1.258	1.4	P102_T00032
P101_T00006	Y	Y	N	1.076	1.1	P103_T00007*
P101_T00007	Y	Y	Y	0.184	1.1	P104_T00002
P102_T00001	Y	Y	N	0.764	0.8	P104_T00003
P102_T00002	Y	Y	N	1.178	1.2	P104_T00004
P102_T00003	Y	Y	N	1.286	1.5	P104_T00005
P102_T00004	Y	N	N		1.4	P104_T00006
P102_T00005	Y	Y	N	1.248	1.3	P104_T00008
P102_T00006	Y	Y	N	1.540	1.6	P104_T00009
P102_T00007	Y	Y	N	0.805	1.0	P104_T00010
P102_T00008	Y	Y	N	1.041	1.1	P104_T00011
P102_T00009	Y	Y	N	0.839	0.9	P104_T00013
P102_T00010	Y	Y	N	0.924	1.0	P104_T00015
P102_T00011	Y	Y	N	1.546	1.6	P104_T00017
P102_T00012	Y	Y	N	1.141	1.2	P104_T00018
P102_T00013	Y	Y	N	0.730	0.8	P104_T00019
P102_T00014	Y	Y	N	1.227	1.3	P104_T00020
P102_T00015	Y	Y	N	1.354	1.4	P104_T00023
P102_T00016	Y	Y	N	1.419	1.5	P105_T00001
P102_T00017	Y	Y	N	0.825	0.9	P105_T00002
P102_T00018	Y	Y	N	1.032	1.1	P105_T00003
P102_T00019	Y	N	N		0.9	P105_T00004
P102_T00020	Y	Y	N	1.309	1.4	P105_T00005
P102_T00021	Y	Y	N	1.508	1.6	P105_T00006

Experiment Name	Ignition (Y/N)	Post Processing (Y/N)	DDT (Y/N)	Measured Equivalence Ratio	Intended Equivalence Ratio	Experiment Name (within ±0.035 error of phi)
P102_T00022	Y	Y	N	1.399	1.5	P105_T00007
P102_T00023	Y	Y	N	0.947	1.0	P105_T00008
P102_T00024	Y	Y	N	1.223	1.3	P106_T00002*
P102_T00025	Y	Y	N	0.704	0.8	P106_T00003*
P102_T00026	Y	Y	N	0.701	1.1	P106_T00004*
P102_T00027	Y	Y	N	1.110	1.2	P107_T00002
P102_T00028	Y	Y	N	1.234	1.3	P107_T00003
P102_T00029	Y	Y	N	0.923	1.0	P107_T00006
P102_T00030	Y	Y	N	1.326	1.4	P107_T00007
P102_T00031	Y	N	N		1.2	P107_T00008
P102_T00032	Y	Y	N	1.605	1.6	P107_T00009
P102_T00033	Y	Y	N	0.675	0.8	P107_T00011
P102_T00034	Y	Y	N	0.844	0.9	P107_T00012
P102_T00035	Y	Y	N	0.083	1.5	P107_T00013
P102_T00036	Y	Y	N	0.475	1.1	P107_T00014
P103_T00001	Y	Y	N	3.084	1.1	P107_T00015
P103_T00002	Y	Y	N	1.055	0.9	P107_T00016
P103_T00003	Y	N	N		1.0	P107_T00017
P103_T00004	Y	N	N		0.8	P107_T00018*
P103_T00005	Y	Y	N	1.368	1.1	P107_T00019
P103_T00006	Y	Y	N	1.438	1.1	P107_T00020
P103_T00007	Y	Y	Y	1.094	1.1	P107_T00021
P103_T00008	Y	Y	N	3.939	1.1	P107_T00022
P104_T00001	Y	N	N		1.1	P107_T00023
P104_T00002	Y	Y	N	0.812	0.8	P107_T00024
P104_T00003	Y	Y	N	1.387	1.4	
P104_T00004	Y	Y	N	1.071	1.1	
P104_T00005	Y	Y	N	1.165	1.2	
P104_T00006	Y	Y	N	1.003	1.0	

Experiment Name	Ignition (Y/N)	Post Processing (Y/N)	DDT (Y/N)	Measured Equivalence Ratio	Intended Equivalence Ratio	Experiment Name (within ±0.035 error of phi)
P104_T00007	Y	Y	N	1.676	1.6	
P104_T00008	Y	Y	N	1.272	1.3	
P104_T00009	Y	Y	N	1.494	1.5	
P104_T00010	Y	Y	N	0.884	0.9	
P104_T00011	Y	Y	N	1.089	1.1	
P104_T00012	Y	Y	N	0.950	0.9	
P104_T00013	Y	Y	N	1.625	1.6	
P104_T00014	Y	Y	N	0.496	1.2	
P104_T00015	Y	Y	N	0.798	0.8	
P104_T00016	Y	Y	N	1.538	1.5	
P104_T00017	Y	Y	N	1.372	1.4	
P104_T00018	Y	Y	N	0.987	1.0	
P104_T00019	Y	Y	N	1.092	1.1	
P104_T00020	Y	Y	N	1.278	1.3	
P104_T00021	Y	N	N		1.5	
P104_T00022	Y	Y	N	1.464	1.3	
P104_T00023	Y	Y	N	1.372	1.4	
P105_T00001	Y	Y	N	1.101	1.1	
P105_T00002	Y	Y	N	1.082	1.1	
P105_T00003	Y	Y	N	1.093	1.1	
P105_T00004	Y	Y	N	1.103	1.1	
P105_T00005	Y	Y	N	1.079	1.1	
P105_T00006	Y	Y	N	1.106	1.1	
P105_T00007	Y	Y	N	1.092	1.1	
P105_T00008	Y	Y	N	1.123	1.1	
P105_T00009	Y	Y	N	1.941	1.1	
P105_T00010	Y	Y	N	1.238	1.1	
P106_T00001	N	N	N		1.1	
P106_T00002	Y	Y	Y	1.098	1.1	

Experiment Name	Ignition (Y/N)	Post Processing (Y/N)	DDT (Y/N)	Measured Equivalence Ratio	Intended Equivalence Ratio	Experiment Name (within ±0.035 error of phi)
P106_T00003	Y	Y	Y	1.130	1.1	
P106_T00004	Y	Y	Y	1.129	1.1	
P107_T00001	Y	N	N		1.4	
P107_T00002	Y	Y	N	1.520	1.5	
P107_T00003	Y	Y	N	0.884	0.9	
P107_T00004	Y	Y	N	1.347	1.3	
P107_T00005	Y	Y	N	1.663	1.6	
P107_T00006	Y	Y	N	1.217	1.2	
P107_T00007	Y	Y	N	1.106	1.1	
P107_T00008	Y	Y	N	1.031	1.0	
P107_T00009	Y	Y	N	0.774	0.8	
P107_T00010	Y	Y	N	1.359	1.3	
P107_T00011	Y	Y	N	0.766	0.8	
P107_T00012	Y	Y	N	1.512	1.5	
P107_T00013	Y	Y	N	1.411	1.4	
P107_T00014	Y	Y	N	0.997	1.0	
P107_T00015	Y	Y	N	1.086	1.1	
P107_T00016	Y	Y	N	0.887	0.9	
P107_T00017	Y	Y	N	1.090	1.1	
P107_T00018	Y	Y	Y	1.103	1.1	
P107_T00019	Y	Y	N	1.088	1.1	
P107_T00020	Y	Y	N	1.093	1.1	
P107_T00021	Y	Y	N	1.082	1.1	
P107_T00022	Y	Y	N	1.094	1.1	
P107_T00023	Y	Y	N	1.085	1.1	
P107_T00024	Y	Y	N	1.086	1.1	

* Experiments with DDT

Appendix C: Maximum peak pressures observed in experiments used for the result analysis

Equivalence ratio	Experiment name	Pressure sensor 1 (bar)	Pressure sensor 2 (bar)	Pressure sensor 3 (bar)	Pressure sensor 4 (bar)
0.8	P107_T00009	2.1	3.7	4.0	4.6
	P107_T00011	2.4	5.6	4.6	4.0
	P104_T00002	3.2	10.3	4.3	6.3
	P104_T00015	2.8	4.6	2.8	5.2
0.9	P107_T00003	2.6	9.1	3.8	7.4
	P107_T00016	2.5	4.9	3.8	8.3
	P104_T00010	2.8	7.7	4.9	6.0
1.0	P107_T00008	2.8	5.8	5.4	8.0
	P107_T00014	2.5	7.8	6.0	9.4
	P101_T00002	2.8	5.5	4.5	11.0
	P104_T00006	2.9	7.1	3.3	7.3
	P104_T00018	3.0	9.3	5.6	6.5
1.1	P107_T00007	3.5	5.2	6.3	8.9
	P107_T00015	3.0	6.5	4.5	9.6
	P107_T00017	2.7	5.8	5.1	6.3
	P107_T00018	3.7	5.4	6.7	18.6
	P107_T00019	2.6	5.9	4.3	10.6
	P107_T00020	3.5	5.3	4.8	9.0
	P107_T00021	3.0	6.1	4.4	9.8
	P107_T00022	3.2	5.1	6.7	8.3
	P107_T00023	2.7	5.2	4.9	7.7
	P107_T00024	3.3	5.3	4.7	8.5
	P106_T00002	3.5	8.9	10.0	21.7
	P106_T00003	4.2	11.6	6.9	17.7
	P106_T00004	3.8	7.8	10.5	21.2

Equivalence ratio	Experiment name	Pressure sensor 1 (bar)	Pressure sensor 2 (bar)	Pressure sensor 3 (bar)	Pressure sensor 4 (bar)
	P101_T00003	3.2	5.1	3.4	5.5
	P101_T00006	3.1	5.0	3.6	5.7
	P103_T00007	4.6	17.3	9.3	37.7
	P104_T00004	3.6	8.0	4.5	9.7
	P104_T00011	3.0	5.6	3.9	9.0
	P104_T00019	3.7	8.7	3.7	10.4
	P105_T00001	3.2	5.0	4.9	7.8
	P105_T00002	3.2	9.5	3.3	8.8
	P105_T00003	3.2	12.3	3.9	7.4
	P105_T00004	4.4	11.9	4.9	8.8
	P105_T00005	3.3	7.2	5.5	11.1
	P105_T00006	3.1	10.1	3.6	9.6
	P105_T00007	3.1	9.2	3.6	7.4
	P105_T00008	3.1	5.3	3.8	8.4
1.2	P107_T00006	2.9	4.7	5.6	6.4
	P102_T00002	3.5	8.9	4.6	7.3
	P104_T00005	3.5	9.4	3.7	8.6
1.3	P104_T00008	2.8	6.2	4.4	8.6
	P104_T00020	3.2	8.0	3.5	8.1
1.4	P107_T00013	2.7	5.8	4.8	7.1
	P104_T00003	2.9	5.0	2.9	7.4
	P104_T00017	3.1	7.7	3.4	7.3
	P104_T00023	3.0	4.8	3.1	5.5
1.5	P107_T00002	2.6	7.5	5.2	4.4
	P107_T00012	3.0	5.1	6.8	5.6
	P104_T00009	3.1	6.8	2.7	5.9

Equivalence ratio	Experiment name	Pressure sensor 1 (bar)	Pressure sensor 2 (bar)	Pressure sensor 3 (bar)	Pressure sensor 4 (bar)
1.6	P102_T00032	3.1	5.0	2.9	5.7
	P104_T00013	2.7	4.8	2.6	4.8

Appendix D: Maximum overpressures observed in channel section one

Equivalence ratio	Experiment name	Peak overpressure	Average
0.8	P107_T00009	0.55	0.55
	P107_T00011	0.52	
	P104_T00002	0.58	
	P104_T00015	0.55	
0.9	P107_T00003	0.68	0.68
	P107_T00016	0.71	
	P104_T00010	0.64	
1.0	P107_T00008	0.77	0.78
	P107_T00014	0.79	
	P101_T00002	0.80	
	P104_T00018	0.78	
1.1	P107_T00007	0.80	0.79
	P107_T00015	0.80	
	P107_T00017	0.80	
	P107_T00018	0.78	
	P107_T00019	0.77	
	P107_T00020	0.78	
	P107_T00021	0.78	
	P107_T00022	0.79	
	P107_T00023	0.78	
	P107_T00024	0.77	
	P106_T00002	0.79	
	P106_T00003	0.80	
	P106_T00004	0.79	
	P101_T00003	0.68	
	P101_T00006	0.69	

Equivalence ratio	Experiment name	Peak overpressure	Average
	P103_T00007	0.82	
	P104_T00004	0.81	
	P104_T00011	0.80	
	P105_T00001	0.82	
	P105_T00002	0.81	
	P105_T00003	0.80	
	P105_T00004	0.82	
	P105_T00005	0.81	
	P105_T00006	0.81	
	P105_T00007	0.80	
	P105_T00008	0.81	
1.2	P107_T00006	0.79	0.79
	P102_T00002	0.79	
	P104_T00005	0.80	
1.3	P104_T00008	0.80	0.79
	P104_T00020	0.78	
1.4	P107_T00013	0.76	0.76
	P104_T00003	0.76	
	P104_T00017	0.77	
	P104_T00023	0.74	
1.5	P107_T00002	0.71	0.72
	P107_T00012	0.73	
1.6	P102_T00032	0.70	0.68
	P104_T00013	0.66	